Feasibility of a weakly intrusive Generalized Finite Element Method implementation in a commercial code: Application to Ceramic Matrix Composite micro-structures

Thomas-David Jayet, Emmanuel Baranger, Guillaume Couégnat, Sébastien Denneulin

Feasability of a weakly intrusive Generalized Finite Element Method implementation in a commercial code: application to Ceramic Matrix Composite micro-structures

Thomas-David Jayet[a,b], Emmanuel Baranger[a], Guillaume Couegnat[c], Sébastien Denneulin[b]

[a] *Université Paris-Saclay, ENS Paris-Saclay, CNRS, LMT - Laboratoire de Mécanique et Technologie, 94235, Cachan, France*
[b] *Safran Ceramics, 105 avenue Marcel Dassault, 33700 Mérignac, France*
[c] *LCTS, Université de Bordeaux , CNRS , CEA , Safran Ceramics, 3 allée de la Boétie, 33600 Pessac, France*

Abstract

In this contribution is addressed the issue of modeling a SiC/SiC composite micro-structure at the fiber scale with elementary features. As the development of new grades of Ceramic Matrix Composites (CMC) for civil aviation grows, different manufacturing processes are used successively and lead to different types of micro-structures and a variable material quality. Consequently a versatile model should be developed in order to compare these materials and create a tool to help engineers to predict the mechanical behavior at the fiber scale. Here the Generalized Finite Element Method (GFEM) is proposed which consists in enriching the classical Finite Element (FE) approached displacement by numerical functions to deliver an accurate description of the fiber-scale structure while limiting the number of degrees of freedom compared to a classical finite element description. A pattern-based description of the microscale is depicted using an industrial code for an engineering purpose. Four main difficulties are highlighted (i) the choice of the enrichment functions regarding the literature (ii) their stiffness matrix computation in a commercial code (iii) the construction of the pattern-based structure and (iv) the post-processing. Two GFEM strategies are presented and demonstrate the feasibility of an enriched kinematics within a classical finite element modeler. The selection of such modeler

is conditioned by the possibility of weakly intrusive automation of the various stages of construction of the enriched patterns with the help of an external scripting language.

Keywords: GFEM, Handbook problem, Implementation, Composites

---

1. Introduction

Ceramic Matrix Composites are good candidates for the aeronautic or the nuclear industries due to their high refractoriness, their low density and their resistance to oxidation compared to metals. In the specific application of gas turbine engines for aviation propulsion, the research of high temperature performance is motivated by a desire of reducing fuel consumption. Indeed a weight loss is not the only motivation for integrating CMCs within hot parts: elevating the operating temperatures of the gas turbine engines enables a gain in propulsion efficiency [1]. Improvements in temperature capabilities allowed an increasing work under service conditions of approximately 35°C per decade [2] in the past.

CMC research has led to the development of various manufacturing processes that have resulted to the creation of several types of structures with different thermal and mechanical properties. For chosen components, two factors have an influence on the thermomechanical behavior: the architecture of the textile reinforcement with unidirectional plies [3], 2D or 3D fabrics [4, 5] and the matrix deposition process. Typically four types of processes can be used for the matrix deposition: the Chemical Vapor Infiltration (CVI), the Chemical Vapor Deposition (CVD), the Melt Infiltration (MI) and the Polymer Impregnation and Pyrolisis (PIP). The chemical vapor processes are employed for a thickness-controled preform coating [6] at the cost of a high porosity rate [7] and a long deposit time. They also can be used to lay an interphase coating such as Pyro-Carbon (PyC) or Boron Nitride (BN) around the fibers. MI and PIP come as a complement to fill the residual porosities (see Fig. 1) and accelerate the matrix deposition. A review of the different manufacturing processes is available in [8]. In particular the matrix deposition processes lead to different micro-structures.

Furthermore many studies have been conducted at the fiber scale in order to quantify the first damages that lead to the material ruin. Degradation mechanisms like fiber debonding [9], fiber cracking due to oxidation [10] and creep [11, 12] have been observed. Silicon Carbide (SiC) textile and matrix (SiC/SiC)

composites behavior under quasi-static indentation [13] or low velocity impact [14] have been observed through micrographic or tomographic studies in order to analyze the damages at the yarn scale. Initial state is also of importance since the post-processing cooling implies a residual stress [15, 16] due to different values of the expansion coefficient for the different phases of the micro-structure [17].

The succession of possible manufacturing processes coupled with the existence of non linear phenomena such as degradation mechanisms at the micro-scale raises the issue of a modeling strategy to predict CMCs behavior and compare solutions for different configurations and loads.

Models for Ceramic Matrix Composites at the fiber scale have been developed for computational applications like crack initiation and propagation criteria [18, 19] or environmental effects modeling [20]. However, the simulation of such phenomena requires the development of calculation tools whose effectiveness depends on the quality of the description of the structure. Thus an adapted strategy for the micro-structure description must be implemented upstream to facilitate the mechanical modeling. For an industrial purpose such modeling method must be implemented in a commercial code so the following developments are chosen to be made with the Abaqus 6.14 software.

The aim of the following paragraphs is to introduce classical strategies used to model composites numerically. A review of the homogenization and domain decomposition strategies is proposed with the purpose of contextualizing the chosen method which will be precised further.

Homogenization consists in averaging quantities such as stresses and strains within a heterogeneous Representative Volume Element (RVE) whose definition can be found in [21]. A satisfying RVE must be statistically representative which implies an upstream study of the volume fraction of the different constituents within the RVE and their allocation. It must have a small characteristic length compared to the macrostructure dimensions so the RVE is assumed to be homogeneous at the macroscale. For non linear investigations applied to periodic RVE, iterative methods based on an asymptotic homogenization [22] applied

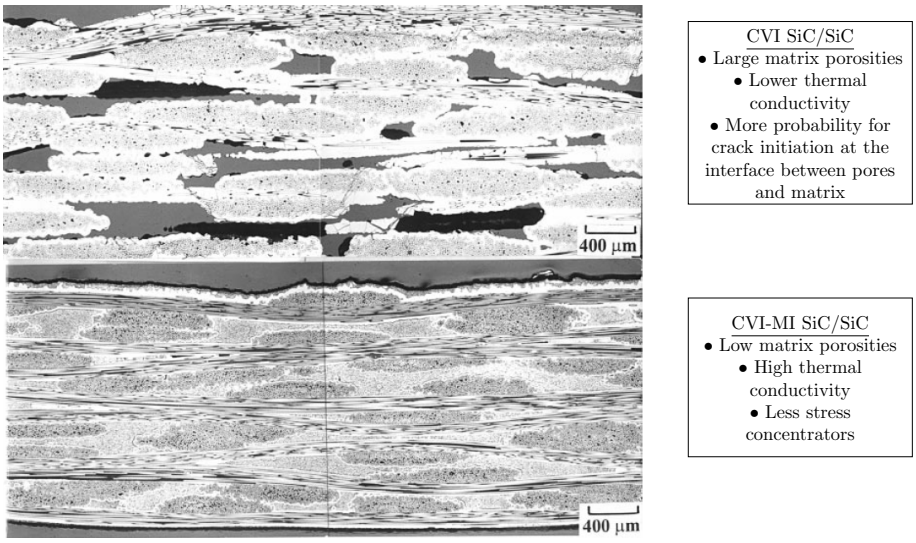

Fig. 1. Comparison between two yarn-scaled structures obtained with a CVI or a CVI-MI process for a SiC-fiber and SiC-matrix (SiC/SiC) composite. Hybrid CVI and MI process results in a fully dense matrix. Micrography from [7].

to coupled scales (reviewed in [23]), FE^2 [24] or Fast Fourier Transform [25] have been suggested for composite applications. However these homogenization strategies suffer from the simplifying assumption of periodicity and uncoupled global-local methods encounter significant errors in the portions with high gradients. Moreover no solution for the micro-structure description is provided and the information to be given is too rich compared to the information at the end of the operation, then homogenization has a limited interest for this study.

Domain Decomposition Methods (DDM) enable to split a global structure into non-overlapping substructures and interfaces. Consequently they allow a fine description of a large structure due to a parallelized computation of the different submodels. Then computation is made with accuracy. Studies have been conducted for laminate composites submitted to time-dependant mechanisms [26, 27]. A crack propagation has also been performed using a hybrid eXtended FEM and DDM formulation [28]. Nonetheless DDM have limitations concerning the sorting of extracted information caused by the accuracy of the

computation. Indeed the output information may be too rich to enable an impact on the selection of the manufacturing processes. Consequently the desired versatility for the composite depiction seems lost.

In addition to the Galerkin formulation, other kinematics descriptions are possible to approach the real displacement. The Superposition Finite Element Method (S-FEM) [29], the Variable size h and Polynomial degree p called hp-adaptivity [30] are some examples. The Partition of Unity Method [31] can be seen as a generalization of the hp-adaptivity and constitutes the foundation of the Generalized Finite Element Method (GFEM) [32]. The key point of the GFEM is to enrich the kinematics with enrichment - also called *special* - functions in order to describe a structure and its behavior on each element patch of the mesh.

The GFEM is a method halfway between those of homogenization and those of HPC. Indeed, an upstream calculation allows to generate patterns on a macroscopic scale from a local description before storing the solutions in a *Handbook*. The enrichment functions enable to keep a coupling between the micro scale and the macro scale. The problem to be solved is then broken down into patterns but the calculation is done in a monolithic way.

For that reason Section 2 of this contribution emphases the Generalized Finite Element Method as a Partition of Unity Method and underlines the difficulties of the method. Then three GFEM implementation strategies are presented in Section 3. Section 4 draws the statement of the tools available in Abaqus in order to estimate the most relevant strategy to implement. Eventually Section 5 presents a weakly intrusive implementation of the GFEM with the help of Abaqus and Python in the particular case of an elastic problem. The novelty of the presented method do not lies in the numerical enrichments generation or the choice of the patterns but in their use in a commercial software. It will be shown that the feasibility of the implemented method is easily automatable through a scripting language.

2. Generalized Finite Element Method

The following section draws a state of the art of the GFEM. Strategies of kinematics enrichment generation are summarized from the literature and discussed in order to select the most appropriate for an easy implementation.

2.1. Problem definition

A domain denoted Ω is considered. Boundary conditions can be applied on $\partial\Omega = \partial\Omega_F \oplus \partial\Omega_u$ as:

$$\underline{\underline{\sigma}}.\boldsymbol{n} = \boldsymbol{F_d} \text{ on } \partial\Omega_F \tag{1}$$

$$\boldsymbol{u} = \boldsymbol{u_d} \text{ on } \partial\Omega_u \tag{2}$$

Where $\boldsymbol{n}$ is the outward unit normal vector to $\partial\Omega_F$ and $\underline{\underline{\sigma}}$ is the Cauchy stress tensor. Such Ω domain is approached by a mesh denoted Ω_h. Centered on the node number k can be defined a patch of elements Ω_k. An illustration of the model problem definition is available in Fig. 2. The strain is assumed to be small and given by the symmetric gradient of the displacement $\boldsymbol{u}$:

$$\underline{\underline{\epsilon}}(\boldsymbol{u}) = \frac{1}{2}\left(\underline{\underline{\nabla}}(\boldsymbol{u}) + \underline{\underline{\nabla}}(\boldsymbol{u})^T\right) \tag{3}$$

For the heterogeneous material the Hooke's elasticity tensor at the coordinate $\mathbf{x}$ denoted $\mathbf{H}(\mathbf{x})$ can be broken down as the sum of a homogeneous part $\mathbf{H}_0$ and a perturbation part $\Delta\mathbf{H}(\mathbf{x})$ such as:

$$\forall \mathbf{x} \in \Omega,\ \mathbf{H}(\mathbf{x}) = \mathbf{H}_0 + \Delta\mathbf{H}(\mathbf{x}) \tag{4}$$

Then the stress tensor $\underline{\underline{\sigma}}$ is linked to the strain tensor by:

$$\underline{\underline{\sigma}}(\mathbf{x}) = \mathbf{H}(\mathbf{x}) : \underline{\underline{\epsilon}}(\boldsymbol{u}) \tag{5}$$

Defining $\mathcal{U}_0 = \{\boldsymbol{u}^* \in \mathrm{H}_1(\Omega)^3, \boldsymbol{u}^* = 0 \text{ on } \partial\Omega_u\}$ and $\mathcal{U} = \{\boldsymbol{u} \in \mathrm{H}_1(\Omega)^3, \boldsymbol{u} = \boldsymbol{u_d} \text{ on } \partial\Omega_u\}$ enable to write the Principle of Virtual Work which reads: Find $\boldsymbol{u} \in \mathcal{U}$ such that $\forall \boldsymbol{u}^* \in \mathcal{U}_0$,

$$-\int_\Omega \underline{\underline{\epsilon}}(\boldsymbol{u}) : \mathbf{H}(\mathbf{x}) : \underline{\underline{\epsilon}}(\boldsymbol{u}^*) d\Omega + \int_{\partial\Omega} \boldsymbol{F_d}.\boldsymbol{u}^* d(\partial\Omega) = 0 \tag{6}$$

2.2. Partition of unity

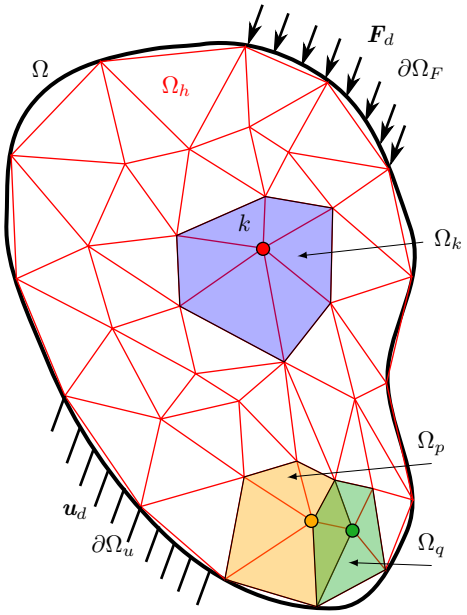

Fig. 2. Exemple of *patches* constitutive of a mesh Ω_h approaching a real structure Ω, subject to load boundary conditions F_d on boundary $\partial\Omega_F$ and displacement boundary conditions u_d on boundary $\partial\Omega_u$.

Based on the Partition of Unity (PU) hypotheses [31], the GFEM formulation suggested in [32] enables to write the displacement approximation as the sum of the regular Finite Element (FE) interpolation and an enriched contribution. In a point $\mathbf{x}$ of the studied domain, such a displacement $\boldsymbol{u}_h(\mathbf{x})$ is written

as presented in (7).

$$\boldsymbol{u}_h(\mathbf{x}) = \underbrace{\sum_{k=1}^{N} \varphi_k(\mathbf{x})\boldsymbol{u}_k}_{\text{FE interpolation}} + \underbrace{\sum_{k=1}^{N} \varphi_k(\mathbf{x}) \sum_{j=1}^{n_{enr}^{(k)}} \psi_k^{(j)}(\mathbf{x})\boldsymbol{a}_k^{(j)}}_{\text{enriched contribution}} \tag{7}$$

N is the number of element patches inside the mesh representing the studied structure, φ_k is the same "hat" function as defined in the classic Finite Element Method (FEM) for the element patch number k called Ω_k and illustrated in Fig. 2, $\boldsymbol{u}_k$ is the displacement vector calculated at the node number k, $n_{enr}^{(k)}$ is the number of enrichment functions inside the patch number k, $\psi_k^{(j)}$ is the enrichment function number j associated with the patch Ω_k and $\boldsymbol{a}_k^{(j)}$ is the additionnal nodal unknown associated with the enrichment number j of Ω_k. It has been shown in [31] that the richer the enrichment functions, the closer the approached displacement $\boldsymbol{u}_h$ is to the exact displacement $\boldsymbol{u}$. The immediate consequence is the emancipation of an explicit mesh due to the presence of features within the micro-structure, thanks to the enrichment functions $\psi_k^{(j)}$. The $\varphi_k\psi_k^{(j)}$ products ensure the continuity of the fields between two superimposed or adjacent patches.

2.3. XFEM and GFEM

A distinction between the Extended Finite Element Method (XFEM) and the GFEM is made in this contribution: despite both of the two strategies are consequences of the PU hypotheses, the first method will designate the extension of the standard FE with analytical enrichments and the second one will refer to the use of numerical special functions.

The XFEM has already been integrated into commercial softwares and is principaly used to model the position and the propagation of cracks by using *level-set* functions and adding a set of tip functions at the crack fronts explicited in [33]. These tip functions are defined from the asymptotic displacement solution and determine the crack deflection. A modified Partition of Unity using Shepard analytical functions [34] was also suggested to describe a crack in a

homogeneous field [35] or to treat problems with multiple junctions in polycristalline structures under thermal loads [36]. It can be noted that the XFEM has been used in Abaqus to model crack deflection at the interface between the matrix and the fiber interphase [37]. A homemade code also made it possible to perform crack propagation in a homogenized composite structure via XFEM using the abaqus modeler [38]. Many studies [39, 40, 41, 42, 43] have been lead in order to improve the implementation and the stability of the method. Nonetheless two limitations of the analytic description of a crack can be highlighted. First the asymptotic displacements used as crack tip enrichment functions are generally valid in an infinite homogeneous domain. Second *level-set* functions give a rough approximation of a crack path if a coarse mesh is used (see Fig. 3), then element partitioning is required since usual Gauss quadrature is only accurate for polynomials. Moreover a multi-material domain demands a fine mesh in order to take into account the structural details which can be small within CMCs micro-structures (such as residual porosities for instance). The XFEM is able to describe a weak discontinuity as a frontier between two materials but it would demand a large number of additional nodal unknowns to describe the whole micro-structure. The GFEM seems to be more flexible due to the numerical enrichment functions, for instance a 3D model of a crack has been treated in [44] avoiding asymptotic expansion of the elasticity solution required in XFEM through the help of a local description of the crack by a geometrically conforming refined mesh. The number of structural details delivers mesh complication as noted in [45] and GFEM can potentially overcome such issue. The difficulty of treating numerous structural details were also overcome [46]. Proper Orthogonal Decomposition (POD) modes were used as GFEM enrichment functions [47]. More recently a Proper Generalized Decomposition (PGD) enrichment generation strategy adapted to transient problems has been developped [48] and allows an off-line storage of the enrichment functions which can be seen as a *Handbook* problem defined in [45, 46]. The *Handbook* classifies pre-calculated patterns used as numerical enrichment functions like a library of features. The main idea of this method is the richer the *Handbook*, the more

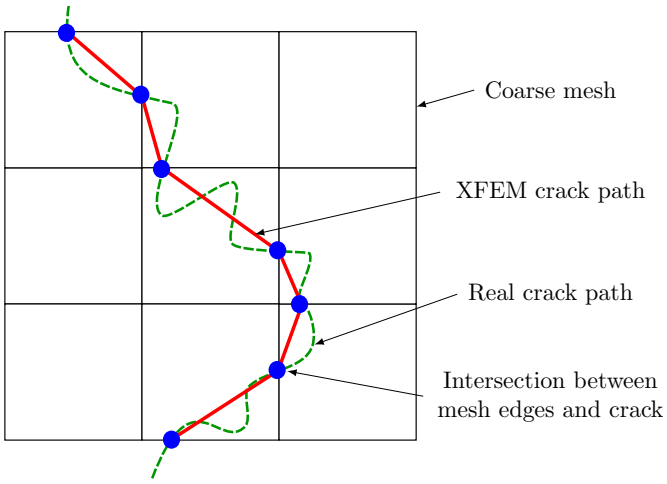

Fig. 3. Crack approximation due to XFEM *level-set* functions.

scenarios and structures can be described.

Before introducing the different implementation strategies existing in the literature, a review of the difficulties associated with the enrichment functions generation is proposed in the following section.

2.4. Difficulties associated with the GFEM and its implementation

The aim of this paper is to present the implementation of a versatile model through the Abaqus software. Such commercial code uses a classical finite element description of the kinematics so the first difficulty is the next:

1. The approached displacement (7) must be imposed on the mesh Ω_h using classical kinematic description tools.

Another point of the implementation of the GFEM is to build the stiffness matrix with regard to the displacement formulation. The virtual work of the internal forces $\int_\Omega \underline{\underline{\epsilon}}(\boldsymbol{u}_h) : \mathbf{H}(\mathbf{x}) : \underline{\underline{\epsilon}}(\boldsymbol{u}_h^*) d\Omega$ with $\boldsymbol{u}_h^* \in \mathcal{U}_0$ provides the form of the stiffness matrix (8) and its components (9).

$$\mathbf{K}_{GFEM} = \begin{pmatrix} \mathbf{K}_{FEM} & \mathbf{K}_{FEM/enr} \\ \mathbf{K}_{FEM/enr}^T & \mathbf{K}_{enr} \end{pmatrix} \tag{8}$$

$$(\mathbf{K}_{FEM})_{IJ} = \int_{\Omega_I \cap \Omega_J} \mathbf{H}(\mathbf{x}) \nabla(\varphi_I) \nabla(\varphi_J) d\Omega \tag{9a}$$

$$(\mathbf{K}_{FEM/enr})_{I\alpha} = \int_{\Omega_I \cap \Omega_p} \mathbf{H}(\mathbf{x}) \nabla(\varphi_I) \nabla(\varphi_p \psi_p^{(k)}) d\Omega \tag{9b}$$

$$(\mathbf{K}_{enr})_{\alpha\beta} = \int_{\Omega_p \cap \Omega_q} \mathbf{H}(\mathbf{x}) \nabla(\varphi_p \psi_p^{(k)}) \nabla(\varphi_q \psi_q^{(l)}) d\Omega \tag{9c}$$

Indices α and β are explicited in (10) and a reminder of the development used to obtain these different terms is available in Appendix 1.

$$\alpha = \sum_{m=1}^{p-1} n_{enr}^{(m)} + k \; ; \; \beta = \sum_{n=1}^{q-1} n_{enr}^{(n)} + l \tag{10}$$

The question of the GFEM stiffness matrix conditioning has been raised [49]. If $\mathcal{R}(\mathbf{A})$ denotes a scaled condition number of a matrix $\boldsymbol{A}$ and $h << 1$ is the characteristic length of the mesh then (11) is verified and highlights the ill-conditioned GFEM stiffness matrix compared to the classical FEM stiffness matrix.

$$\frac{\mathcal{R}(\mathbf{K}_{FEM})}{\mathcal{R}(\mathbf{K}_{GFEM})} = \mathcal{O}(h^2) \tag{11}$$

As a consequence convergence of an iterative solution method may be deteriorated. Modified enrichment functions have been used in order to correct the ill-conditioning of the GFEM stiffness matrix and reach the same order than $\mathcal{R}(\mathbf{K}_{FEM})$. This result is obtained by deleting the linear part of the enrichment functions from a patch [49, 50]. An illustration is shown in Fig. 4, the modified enrichment function $\widehat{\psi}_k^{(j)}$ enables to obtain a condition number of the same order of magnitude as for the FEM one.

The main difficulty associated with the GFEM stiffness matrix is to evaluate the integration of the cross-products $\nabla(\varphi_I)\nabla(\varphi_p \psi_p^{(k)})$ and mainly $\nabla(\varphi_p \psi_p^{(k)})\nabla(\varphi_q \psi_q^{(l)})$ between superimposed patches $\Omega_I \cap \Omega_p$ and $\Omega_p \cap \Omega_q$ respectivelly. Indeed hat functions are associated to the coarse mesh Ω_h while special functions $\psi_k^{(j)}$ potentially come from explicit meshes of support $\omega_k^{(j)}$ describing structural details

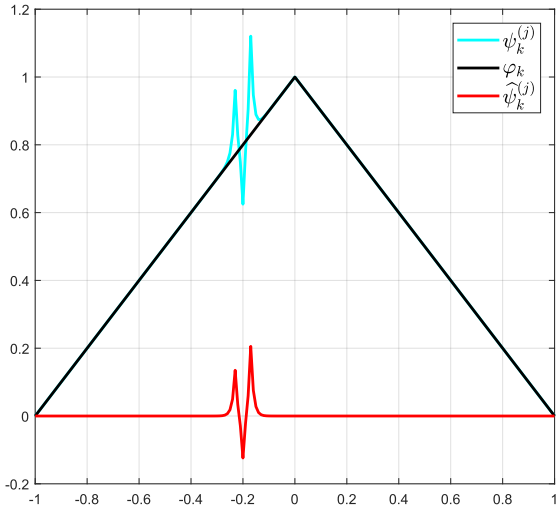

Fig. 4. Construction of a SGFEM enrichment function. The piecewise linear interpolant of the enrichment function is substracted from the enrichment function $\psi_k^{(j)}$ to obtain the SGFEM enrichment function $\widehat{\psi}_k^{(j)}$.

and their behavior. Depending on the description strategy of the local domains $\omega_k^{(j)}$ an integration issue may occur due to non-conforming meshes. Then a refined grid is necessary to project fields or the developpement of an adaptive quadrature can be suggested [45]. However, such an operation requires additional calculations to be performed that require the permanent rewriting of files in a commercial code. The calculation time would potentially become too long, especially in order to deal with non-linear problems in the future. The field projection on a commercial code like Abaqus would therefore undermine the effectiveness of the method proposed in this paper. Consequently the second difficulty to overcome is the next:

2. The integration of cross-products $\nabla(\varphi_p\psi_p^{(k)})\nabla(\varphi_q\psi_q^{(l)})$ in (9) must be simplified.

With the aim of responding to the two difficulties highlighted in this section a review of the different enrichment strategies is suggested in Section 3. Then

an analysis of the Abaqus capacities will be presented in Section 4 in order to help to choose a relevant implementation method using this modeler and weakly intrusive languages such as Python for instance.

3. Enrichment functions generation strategies

This section draws the state of the art of the existing numerical enrichment strategies available in the literature in a chronological order.

3.1. Enrichment by precalculated solutions

A natural idea lies in the generation of enrichment functions coming from a combination of canonic loads illustrated in Fig. 5 and introduced by Strouboulis in [45]. These canonic loads allow these patterns to accommodate a combination of the precalculated loads in an elastic problem. Such precalculated solutions are stored in a *Handbook* and overlaid to a coarse mesh representing the geometry of the homogeneous part of the studied structure. A Computer-Assisted Design (CAD) representation is required so that the geometry of the *Handbook* problems can be extracted and meshed. Nonetheless the nonconformity between superimposed meshes implies a step of field interpolation and the difficulties in the calculus of the cross-products introduced in (9). A heavy adaptive procedure has been developped [45] to solve that non-conforming problem.

3.2. Enrichment by geometrically conforming meshes

Each macroscopic patch which contains a structural detail such as cracks, porosities, fibers or other observable phases of the composite micro-structure must be enriched. The main idea of this strategy later called Duarte's method is to impose the GFEM kinematics to the macroscopic nodes of a patch knowing the local behavior within. To simplify the cross-products for superimposed patches a refined mesh containing the structural details is added to the entire coarse global mesh in order to ensure the geometric conformity between the patches then to guarantee the same local description at the intersection between

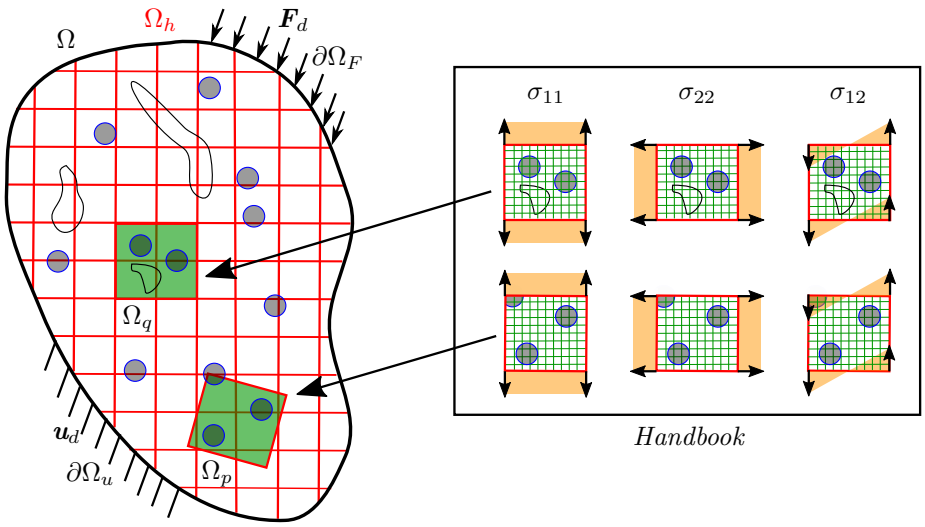

Fig. 5. Enrichment generation by load base: patterns are chosen from a homogeneous structure. A canonic load base applied on a refined mesh including structure details is used to calculate numerical enrichment functions. Then such patterns can be superimposed to the global structure to approach the desired model.

two patches. Moreover for the patch Ω_p, one enrichment function $\psi_k^{(p)}$ associated with the "hat" function φ_k is computed following at a point $\mathbf{x}$:

$$\psi_k^{(j)}(\mathbf{x}) = \boldsymbol{u}_{tot}^{(j)}(\mathbf{x}) - \boldsymbol{u}_{hom}^{(j)}(\mathbf{x}) \tag{12}$$

$\psi_k^{(j)}(\mathbf{x})$ is the difference between the displacement $\boldsymbol{u}_{tot}^{(j)}(\mathbf{x})$ obtained for the real behavior and the displacement $\boldsymbol{u}_{hom}^{(j)}(\mathbf{x})$ calculated for the global homogeneous behavior at the local scale: it is seen as a perturbation contribution of the homogeneous displacement field. By construction such enrichment functions respect the SGFEM. Eventually the created features stored in the *Handbook* are reinjected in the global model as shown in Fig. 6.

3.3. Enrichment by scale separation

In addition to the partition of unity hypotheses, scale separation hypotheses have been introduced in [51] and withdrawn below:

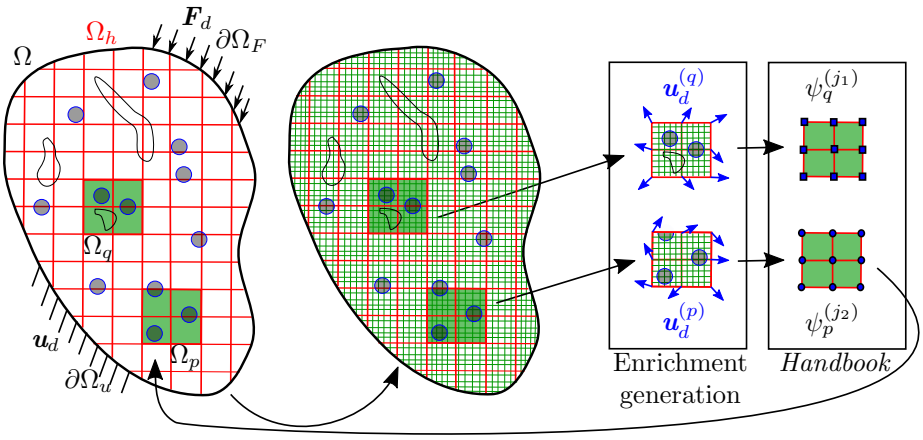

Fig. 6. Illustration of the different steps to fill the *Handbook*. First a simulation is performed on a macroscopic coarse mesh (at the left). Secondly a geometrically conforming local mesh is generated in the whole structure. Then patches are extracted to compute the special functions before their reinjection in the model.

1. The support $\omega_k^{(j)}$ of the enrichment function $\psi_k^{(j)}$ is small in comparison with the support Ω_k of the hat function φ_k
2. The enrichment functions do not interact with each other.

The first assumption can be interpreted as the hat functions φ_k are almost constant on the support $\omega_k^{(j)}$, so if $\mathbf{C}_k^{(j)}$ is the center of $\omega_k^{(j)}$ it can be written:

$$\varphi_k(\mathbf{x}) \approx \varphi_k(\mathbf{C}_k^{(j)}) \ \forall \mathbf{x} \in \omega_k^{(j)} \tag{13}$$

The second assumption results in an empty intersection between two different enrichment supports. Since the enrichment functions are located on a support $\omega_k^{(j)}$ with a center $\mathbf{C}_k^{(j)}$ a modified then by setting $\widetilde{\psi}_k^{(j)} = \varphi_k(\mathbf{C}_k^{(j)})\psi_k^{(j)}$ the approached displacement (7) can be simplified and written as shown in (14).

$$\widetilde{\boldsymbol{u}}_h(\mathbf{x}) = \sum_{k=1}^{N} \varphi_k(\mathbf{x})\boldsymbol{u}_k + \sum_{k=1}^{N}\sum_{j=1}^{n_{enr}^{(k)}} \widetilde{\psi}_k^{(j)}(\mathbf{x})\boldsymbol{a}_k^{(j)} \tag{14}$$

It can be noted that the enrichment contribution is independent from the hat functions. Consequently the additional nodes $\boldsymbol{a}_k^{(j)}$ can be placed anywhere

within the patch. As a convention the additional nodes $\boldsymbol{a}_k^{(j)}$ will be located at the centers $\mathbf{C}_k^{(j)}$ of the enrichment supports $\omega_k^{(j)}$.

Moreover the terms of the associated stiffness matrix can be calculated similarly to the demonstration of the GFEM stiffness matrix terms (9) and give:

$$(\mathbf{K}_{FEM})_{IJ} = \int_{\Omega_I \cap \Omega_J} \mathbf{H}(\mathbf{x}) \nabla(\varphi_I) \nabla(\varphi_J) d\Omega \tag{15a}$$

$$(\mathbf{K}_{FEM/enr})_{I\gamma} = \int_{\omega_p^{(k)}} \mathbf{H}(\mathbf{x}) \nabla(\varphi_I) \nabla(\widetilde{\psi}_p^{(k)}) d\Omega \tag{15b}$$

$$(\mathbf{K}_{enr})_{\alpha\beta} = \int_{\omega_p^{(k)}} \mathbf{H}(\mathbf{x}) \nabla(\widetilde{\psi}_p^{(k)}) \nabla(\widetilde{\psi}_p^{(k)}) d\Omega \tag{15c}$$

The issue of cross-products highlighted in (9) is then avoided, more precisely the scale separation hypotheses allow the superimposition of nonconforming meshes used as support of features. The enrichment functions generation strategy using load base described ahead is brought more versatile, at the price of an approached kinematics which does not fully respect the Partition of Unity hypotheses. Nonetheless such simplification is considered sufficient through a development of a comprehension tool [51]. An application in the crack propagation case has been implemented in Castem [52]. To summarize multi-scale GFEM (MS-GFEM) enrichment strategy is close to the load based one and illustrated in Fig. 7. Either a stress or strain basis can be used to generate the numerical enrichment functions. the main difference between the GFEM and the MS-GFEM is the emancipation of interactions between feature supports. It can also be noted that the description of the structure only relies on the precalculated *Handbook* and the enrichment functions as defined in (12) satisfy the SGFEM conditions.

4. Available tools in commercial codes

The following section presents useful Abaqus tools in order to prove the feasability of the different strategies concerning the GFEM implementation in-

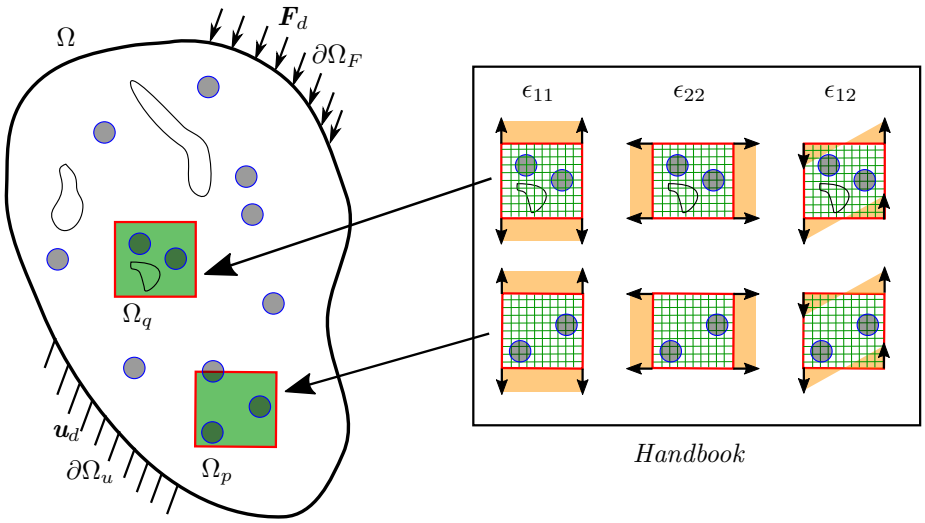

Fig. 7. Enrichment functions patches chosen from the *Handbook* positioned in the global domain to take in account the structural details, regarding the MS-GFEM hypotheses. Here a canonic strain base is used to generate the enrichment functions.

troduced previously. For this section the names of Abaqus functionalities will be written in *Italic*.

4.1. Geometrically conforming meshes

A geometrically conforming refined mesh with a macroscopic one allows a same local description in regards to the intersection of two patches. It would result in a simplification of the cross-products within the GFEM stiffness matrix. Nonetheless only one mesh can be associated with a given CAD structure in Abaqus. Consequently it is not possible to realize a coarse mesh and to superimpose a refined mesh respecting the edges of the macroscopic one. One solution consists in operating a *Partition* on the CAD to draw manually the edges of the global mesh. In a second time the model can be copied and a refined mesh can be generated on the new structure. The partition edges will impose the shape of the local mesh and the conformity with the macroscopic one. It is illustrated with the point ② in Fig. 8.

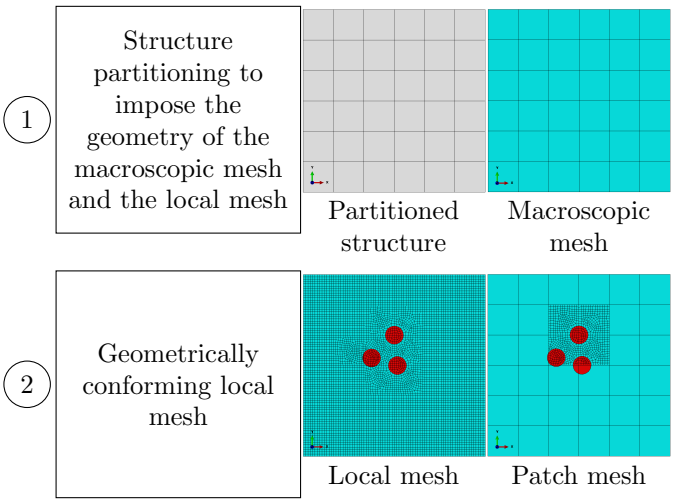

Fig. 8. Structure partitioning. The partition tool imposes the edges in the global structure so the global and local meshes are forced to fit them. Heterogeneous inclusions are highlighted in red. The characteristic size of the global mesh is about a hundred times larger than that of the local mesh.

4.2. Macroscopic kinematics imposed to the local mesh

In the global-local GFEM and the MS-GFEM the numerical enrichment functions can be generated from the local response of the structure to the macroscopic kinematics. Then it is necessary to be able to project the global displacements onto the local mesh. In Abaqus the *Submodeling* tool drives the local model with the results from the global model. An interpolation is then performed to determine the solution of the submodel. For instance the point ① of the Fig. 9 illustrates a hat function of a macroscopic patch. Nodes at the boundary of the patch are fixed and the central one is associated with a unitary displacement. Point ② shows the displacements calculated for the submodel of the patch if the macroscopic kinematics is imposed on the whole surface of the patch.

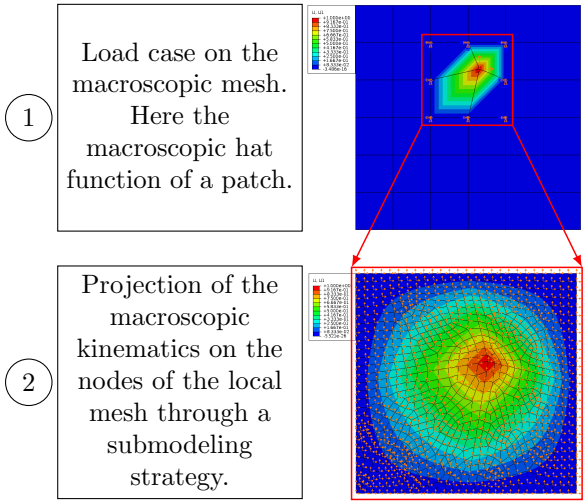

Fig. 9. Projection of a global field on a local mesh through a submodeling strategy. The local mesh is assumed to be a submodel of the macroscopic structure and follows its kinematics. Then each local node is subject to a displacement boundary condition (in orange).

4.3. Enrichment functions seen as perturbation functions

Since the numerical enrichment functions can be seen as a perturbation function between the heterogeneous and the homogeneous structure, the question arises as to how to substract two different displacement fields from two different Abaqus simulations. It is possible to extract the nodal displacements and store them in a Python list for instance. Indeed Python is able to read the Abaqus result file. For instance in the points ① and ② of the Fig. 10 the same macroscopic kinematics is imposed at the boundaries of the homogeneous patch and the heterogeneous patch. The difference between the two displacement field can be made with Python and gives the point ③ if reinjected in Abaqus.

4.4. Imposing the GFEM approached displacement

The GFEM approached displacement (7) must be implemented in Abaqus to replace the Galerkin displacement formulation. If $\boldsymbol{u}_i^{(local)}$ denotes a local nodal displacement at the point $\mathbf{x}_i$ (with $i \in [\![1, N_{local}^{(p)}]\!]$), $\boldsymbol{u}_k$ (with $k \in [\![1, N_{global}^{(p)}]\!]$) is the macroscopic displacement number k and $\boldsymbol{a}_k^{(j)}$ designates the additional nodal

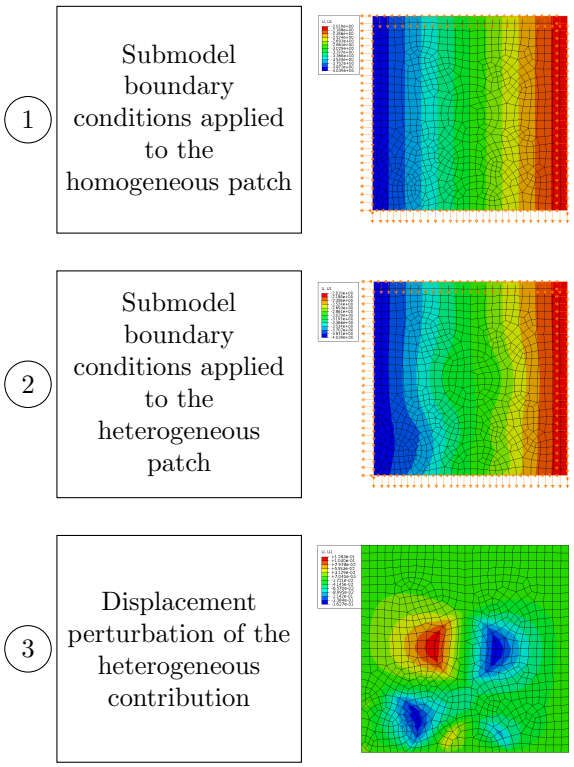

Fig. 10. Numerical enrichment function seen as the perturbation between the heterogeneous response and the homogeneous response to identical boundary conditions.

unknown associated with the enrichment function number j (with $j \in [\![1, n_{enr}^{(p)}]\!]$) then it is possible to impose the GFEM (or the MS-GFEM) kinematics thanks to the *Equation* tool available in the *Constraint* module by writing (here in the case of the GFEM):

$$\boldsymbol{u}_i^{(local)} - \sum_{k=1}^{N_{global}^{(p)}} \varphi_k^{(i)} \boldsymbol{u}_k - \sum_{k=1}^{N_{global}^{(p)}} \varphi_k^{(i)} \sum_{j=1}^{n_{enr}^{(p)}} \psi_k^{(j,i)} \boldsymbol{a}_k^{(j)} = \mathbf{0} \tag{16}$$

Considering a patch Ω_p, $N_{local}^{(p)}$, $N_{global}^{(p)}$ and $n_{enr}^{(p)}$ refer respectively to the number of nodes within the local mesh, the number of nodes within the macroscopic mesh and the number of enrichment functions. $\varphi_k^{(i)}$ indicates the value of the macroscopic hat function interpolated at the coordinate $\mathbf{x}_i$ and $\psi_k^{(j,i)}$ denotes

the value of the enrichment function at the same point $\mathbf{x}_i$. Nodal displacements $\boldsymbol{u}_k$ and enrichment unknown nodes $\boldsymbol{a}_k^{(j)}$ must be added due to the definition of new *Reference Points* in order to be reused for other equation definitions. Indeed Abaqus eliminates the terms used to describe the local displacements $\boldsymbol{u}_i^{(local)}$ for a memory gain purpose. Assimilating the macroscopic nodes with *Reference Points* forbids Abaqus to erase them.

4.5. Substructuring operation with GFEM kinematics

In the GFEM approached displacement (7), unknowns $\boldsymbol{u}_k$ and $\boldsymbol{a}_k^{(j)}$ are defined on macroscopic nodes. Nonetheless the structure behavior is contained in the local description and more particularly in the enrichment functions $\psi_k^{(j)}$. A static condensation will be necessary to integrate the stiffness matrix taking into account the GFEM kinematics. For that purpose the *Substructuring* tool enables an elimination of the internal nodes of a structure and keeps the *Retained Nodal Degrees of Freedom* while ensuring a linear response of the created substructure. The substructuring strategy can work in conjunction with the *Equation Constraint* introduced previously. The local nodes $\boldsymbol{u}_i^{(local)}$ described by the GFEM kinematics are assumed to be the internal nodes of the mesh to be substructured and the macroscopic nodes $\boldsymbol{u}_k$ and $\boldsymbol{a}_k^{(j)}$ are supposed to be the retained nodal degrees of freedom. The *Reference Points* which are necessary in the definition of the *Constraint Equations* can also be associated with retained nodal degrees of freedom. If $\boldsymbol{U}_l$ is the vector containing all the local displacements $\boldsymbol{u}_i^{(local)}$ and $\boldsymbol{U}_b$ is the vector containing all the macroscopic displacements $\boldsymbol{u}_k$ and the enrichment unknowns $\boldsymbol{a}_k^{(j)}$ the linear problem to solve for the patch illustrated in Fig. 11 can be expressed as shown in (17), with $\boldsymbol{f}_l$ and $\boldsymbol{f}_b$ the nodal forces.

$$\begin{pmatrix} \mathbf{K}_{ll} & \mathbf{K}_{lb} \\ \mathbf{K}_{bl} & \mathbf{K}_{bb} \end{pmatrix} \begin{pmatrix} \boldsymbol{U}_l \\ \boldsymbol{U}_b \end{pmatrix} = \begin{pmatrix} \boldsymbol{f}_l \\ \boldsymbol{f}_b \end{pmatrix} \tag{17}$$

As a matter of fact, the set of internal displacements $\boldsymbol{U}_l$ is equal to zero because of the links between the macroscopic displacements and the local ones

established in (16). Consequently the previous system of equations (17) does not need to be solved to find the $\boldsymbol{U}_b$ set. The *Substructuring* tool used in accordance with the *Constraints* (16) simply allows the construction of a macroscopic object with the desired GFEM stiffness matrix.

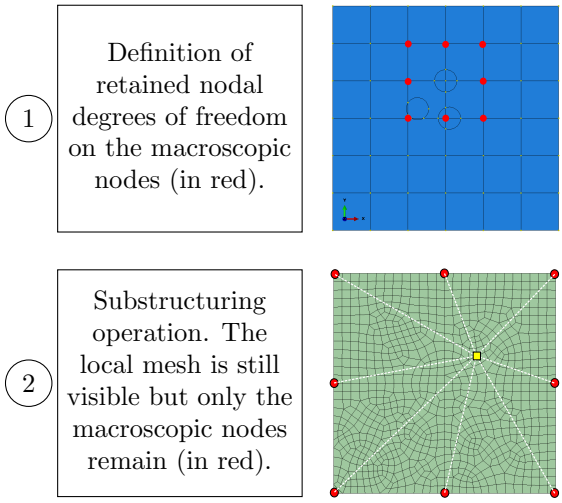

Fig. 11. Substructuring operation. A static condensation is performed in order to express the stiffness matrix on the macroscopic nodes of a patch. The local nodes are represented by the yellow square, the macroscopic nodes by the red circles.

4.6. Patch connection applied to the global-local GFEM

Once the Duarte's enriched patches are generated separately they must be repositioned. Then the difficulty lies in the macroscopic nodes superimposition. Fig. 12 shows two superimposed patches composed of four macroscopic elements each. The enrichment nodes are represented by the square points for one patch and by triangles for the other patch. Macroscopic displacement nodes are represented by the circle points. The common macroscopic element is in red and two circular heterogeneities are drawn. Superimposed nodes schematized by the same geometric shape are assumed to have the same kinematics. The *Tie* tool enables to impose the same displacement between two nodes with the same coordinates.

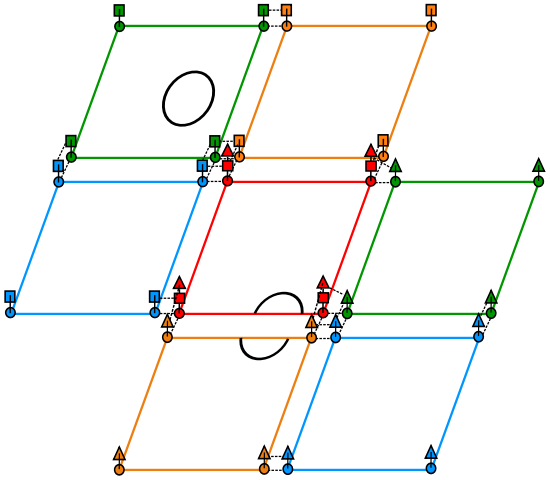

Fig. 12. Two superimposed patches composed of four macroscopic element each. Superimposed nodes with the same geometric shape (circle, square or triangle) are assumed to be equal.

4.7. Substructure positioning in Abaqus

For the specific application to the MS-GFEM, once the enriched patches have been generated and stored in the *Handbook*, the question is how to link them to the macroscopic kinematics of the structure. A natural idea is to superimpose the patches over the global structure as shown in Fig. 13 but two issues can be underlined caused by the enrichment procedure:

1. The stiffness matrix of each patch takes into account the total behavior $\mathbf{H}$ in the finite element part $\mathbf{K}_{FEM}$ in (8)

2. A substructuring operation forbids an interpolation between the macroscopic kinematics and the $\boldsymbol{u}_k$ nodes in each patch

The first difficulty implies a stiffening of the structure because of the superposition of the homogeneous part between the patch and the global structure. Indeed if in the decomposition of behavior $\mathbf{H}$ defined in (4) the homogeneous part corresponds to the silicium MI matrix behavior and $\Delta\mathbf{H}$ is induced by the structural details then the homogeneous behavior is taken into account both in

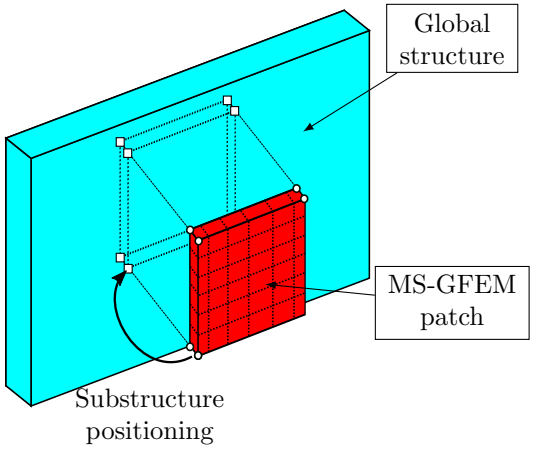

Fig. 13. Superimposition of an enriched patch over a homogeneous global structure.

the finite element part of the GFEM stiffness matrix (15a) and in the homogeneous global structure. Consequently the behavior $\mathbf{H}_0$ must be removed from the finite element part of $\mathbf{K}_{GFEM}$. It is possible by inserting a macroscopic element with the same size as the patch. A negative homogeneous behavior $-\mathbf{H}_0$ is adopted for that element and a master-slave nodes procedure imposes the same nodal displacement between the enriched patch and its finite element support.

An interpolation of the global kinematics must be performed on the features placed to model the desired micro-structure. It is technically possible with Abaqus to interpolate the macroscopic FE kinematics from a mesh to another with the function *Embedded Elements*. So the patch support presented previously enables such operation and avoids the second difficulty highlighted. The patch positioning procedure is illustrated in Fig. 14.

4.8. Partial conclusion: choice of an enrichment strategy

Strouboulis defines a *Handbook* problem. Each precalculated pattern is superimposed over a mesh used as a support. Nonetheless the pre-treatment by adaptive procedure and the constraint imposed by the commercial code Abaqus encourages not to adopt that strategy.

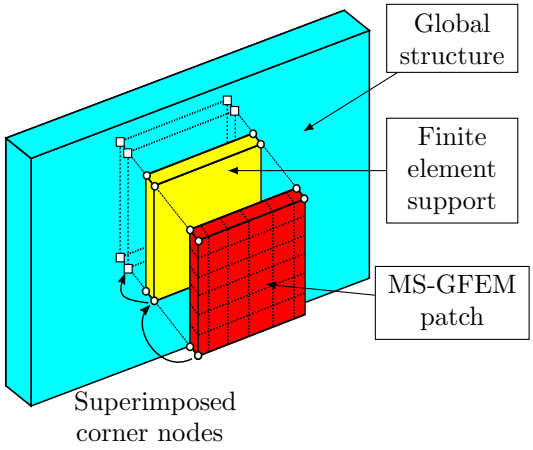

Fig. 14. Superimposition of an enriched patch over an intermediate homogeneous patch with an opposite behavior to compensate the homgeneous one from the global structure.

The Duarte's global-local GFEM approach permits an accurate solution thanks to the respect of the PUM in the GFEM kinematics provided that the local description (and then the mesh size) is fine enough. Moreover the enrichment generation can be parallelized since each patch can be processed independently and patch connections are easy to process. A limitation of this method is that each heterogeneity is taken into account by different enrichment functions due to the local description so the same structural details such as circular fibers with a constant radius are subject to numerous enrichment operations. It also can be noticed that Abaqus requires licenses for each calculus thus a parallelization is potentially greedy[1].

Similarly to the Strouboulis's *Handbook* problem, stored precalculated patterns can be used as enrichment functions and called in the global structure in order to build the desired model. The scale separation hypotheses give the advantage of the mesh independency between the features and the macroscopic support.

[1] If N_{Proc} is the number of processors used for the computation, the number of Abaqus licenses can be deduced from the formula: $5.(N_{proc})^{0.442}$

In terms of Abaqus tools available to write the GFEM kinematics, the enrichment functions can be generated for both the three different strategies introduced previously. Indeed for each presented method a macroscopic load is imposed to the boundaries of the features and allow the numerical calculus of the enrichment function as a perturbation function. The substructuring tool enables local information to be fed back to the scale of the macroscopic patch. The main advantages of the MS-GFEM compared to the global-local strategy is (i) its ability to generate once for all the different enrichment functions and (ii) the possibility to call one pattern many times thanks to the non-interaction hypothesis. Then the MS-GFEM is potentially a low-cost method next to the Duarte's one.

In any case all the previous steps to build the numerical enriched patches can also be automatized with a Python script. It is then possible to process easily all the micro-structures, their behavior, their mesh parameters, the boundary conditions and the nodal displacement collection to generate the enriched patches.

The different Abaqus tools introduced in the current section prove the feasability of the GFEM implementation in Abaqus, with the Duarte and the multiscale point of view. In the following section a numerical example of the multiscale GFEM is presented. A choice not to present an application by geometrically conforming meshes is volontary made due to the high cost of the reading and writing files related to the generation of enrichment functions. Moreover the tools described in Section 4 are the same for the MS-GFEM. Eventually the enrichment functions generation algorithm is summarized in the Appendix 2 in the case of the MS-GFEM.

5. Application of the MS-GFEM

5.1. Reference problem

A micro-structure of CMC is considered. It is composed of 17 Hi-Nicalon^{TM}-S fibers coated with Boron Nitride (BN). The matrix is heterogeneous and composed of a SiC CVI layer complemented with a silicium MI matrix. A

tensile test is performed imposing three surface sliding boundary conditions to prevent rigid body movements and a unitary displacement along direction $\boldsymbol{x}$ as illustrated in Fig. 15.

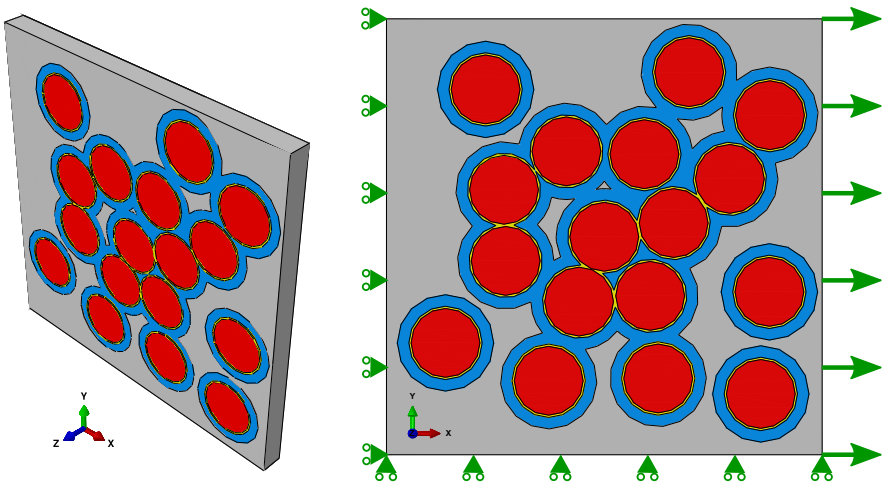

Fig. 15. Reference Element Volume considered. The fibers are colored in red, the BN coating in yellow, the CVI SiC in blue and the Si MI in grey. A hypothesis of plane strain is adopted. A traction load along $\boldsymbol{x}$ is applied with $\boldsymbol{u}_d = 1.\boldsymbol{x}$.

The material properties are summarized in Table 1 and correspond to the HiPerComp® SiC/SiC CMCs [53, 37]. Geometric dimensions are deduced from micrographies in the literature and are given in Table 2. Fibers radius is assumed to be constant and given by the manufacturer [54].

	Young Modulus	Poisson ratio
Hi-Nicalon S fiber	$E_{fib} = 420\ GPa$	$\nu_{fib} = 0.2$
BN interphase	$E_{BN} = 62\ GPa$	$\nu_{BN} = 0.17$
SiC CVI matrix	$E_{SiC} = 400\ GPa$	$\nu_{SiC} = 0.3$
Si MI matrix	$E_{Si} = 165\ GPa$	$\nu_{Si} = 0.3$

Table 1. material properties of interest in this study

Hexahedral elements are adopted in the reference simulation, the thickness

REV Depth	5 μm
REV Side length	$c = 60\ \mu m$
Hi-Nicalon^{TM} -S radius	$R = 6\ \mu m$
BN interphase thickness	$e_{BN} = 0.4\ \mu m$ [55]
SiC CVI thickness	$e_{SiC} = 2\ \mu m$ [56]

Table 2. Dimensions used in this model

of the structure is swept by one element. The FE model contains 524 588 degrees of freedom and only one CPU is used. The first component of the strain tensor is drawn on Fig. 16 with the Matlab software by reading the Abaqus report file containing the strain components at the Gauss points.

5.2. Choice of the features to store in the handbook

In order to recreate the configuration of the reference REV from patterns picked up in a *Handbook* it is necessary to choose such patterns. Different features can be extracted from the observation of the reference REV: single circular inclusion or two close circular inclusions as illustrated in Fig. 17 and introduced in [51]. One inclusion is composed of a Hi-Nicalon^{TM}-S fiber, the BN coating and the CVI SiC matrix. BN coating and CVI SiC matrix can interpenetrate in a multi-circular inclusions pattern. The main objective of this section is to find a criterion in order to choose an enrichment support size denoted c thereafter. In the particular case where the load is plane it is possible to draw inspiration from the work of Lekhnitskii [57]. For one circular inhomogeneity in an infinite plate like illustrated in Fig. 18 the stress field is given analytically according to potential functions and Dundurs's coefficients [58].

Remembering that the composite inclusions are made of several phases, just one material can be retained to use the Lekhnitskii's model. For a given external stress solicitation the higher the rigidity of the inclusion, the more extensive the deformation field around it. Consequently the chosen radius of the circular

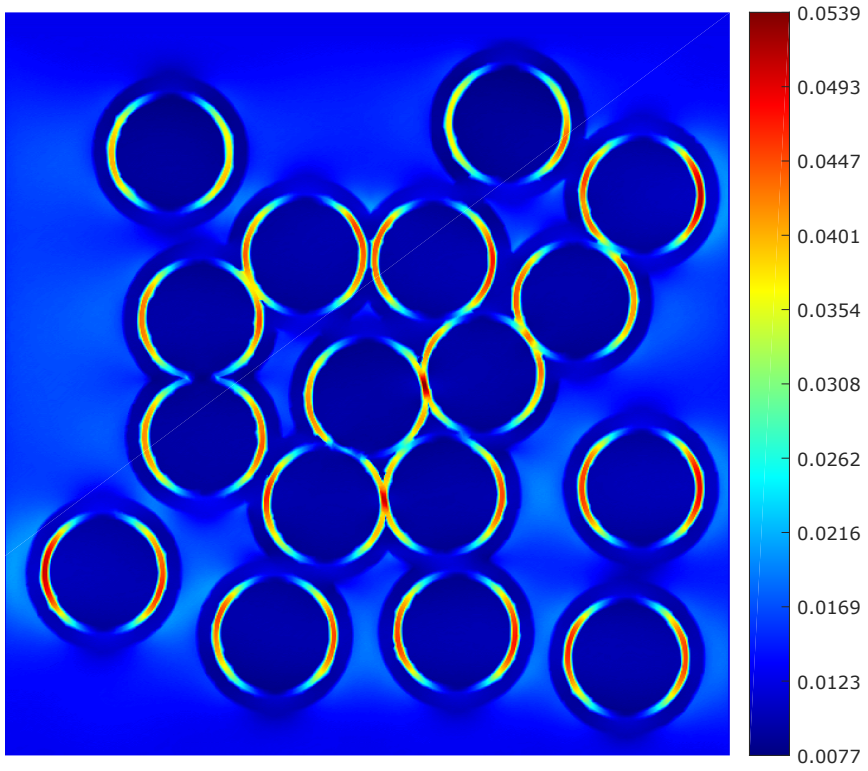

Fig. 16. First component of the strain tensor denoted E_{11} written at the nodes with the Matlab software.

inclusion can be taken equal to $R_{inc} = R + e_{BN} + e_{SiC}$ and its Young modulus can be set at $E_{fib} = 420\ GPa$. If a patch with two fibers must be sized, a circular inclusion embracing the two fibers will be considered. Such choice enables to oversize the patch. Since the patches to be sized must contain as much information as possible about the structure detail that is defined inside, a strain energy criterion is chosen to conclude about the size of each patch. Indeed the knowledge of the analytical strain energy $\omega(\mathbf{x})$ leads to the knowledge of its minimum value reached for an infinite distance of the fiber ω_∞. If $\mathbf{x} = \boldsymbol{0}$ refers to the center of the circular inclusion and c refers to the length of the patch

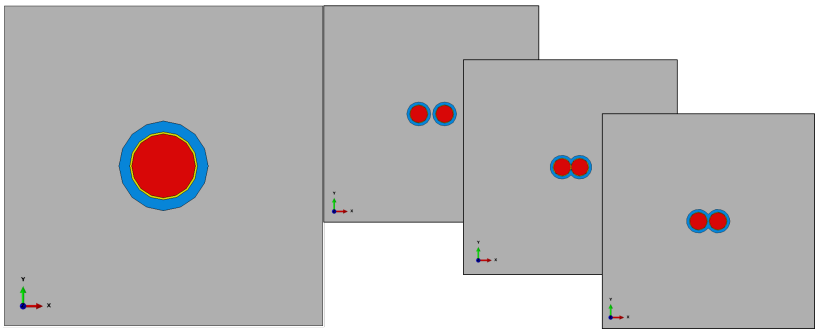

Fig. 17. Examples of patterns extracted from the reference REV. Several features with two fibers must be considered because of the possible different distances between them. The fiber is in red, the interphase is yellow, the CVI matrix is blue and the MI matrix is grey. Each feature is a square of length c which must be dimensioned.

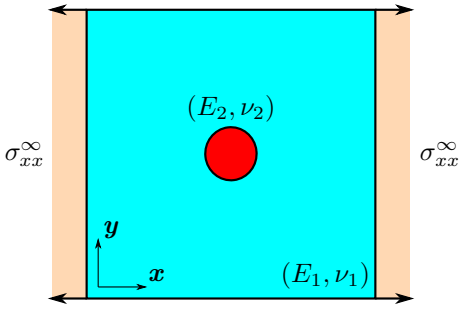

Fig. 18. Lekhnitskii's model for the calculus of the analytical stress field around a circular inclusion (in red) plunged in an infinite homogeneous plate (in blue).

then then the following criterion is defined:

$$\omega\left(\mathbf{x}.\boldsymbol{x} = \frac{c}{2}\right) = (1+\epsilon)\omega_{\infty} \tag{18}$$

Here $\boldsymbol{x}$ is the base vector from Fig. 18, $\mathbf{x}$ is the position within the structure and ϵ is an adjustable setting. For a tensile test along direction $\boldsymbol{x}$ component σ_{xx} is predominant and spreads along the same axis $\boldsymbol{x}$. Fig. 19 shows the evolution of the volumic strain energy along x-axis, for $\epsilon = 10\%$ the chosen relative gap allowed here. For a patch including one fiber the theory leads to a patch size of $c = 60\ \mu m$ which is 10 times the radius of a Hi-Nicalon$^{\text{TM}}$-S fiber. For a patch

including two fibers the maximum size calculated is of $c = 150\ \mu m$ which is 25 times the radius of one fiber.

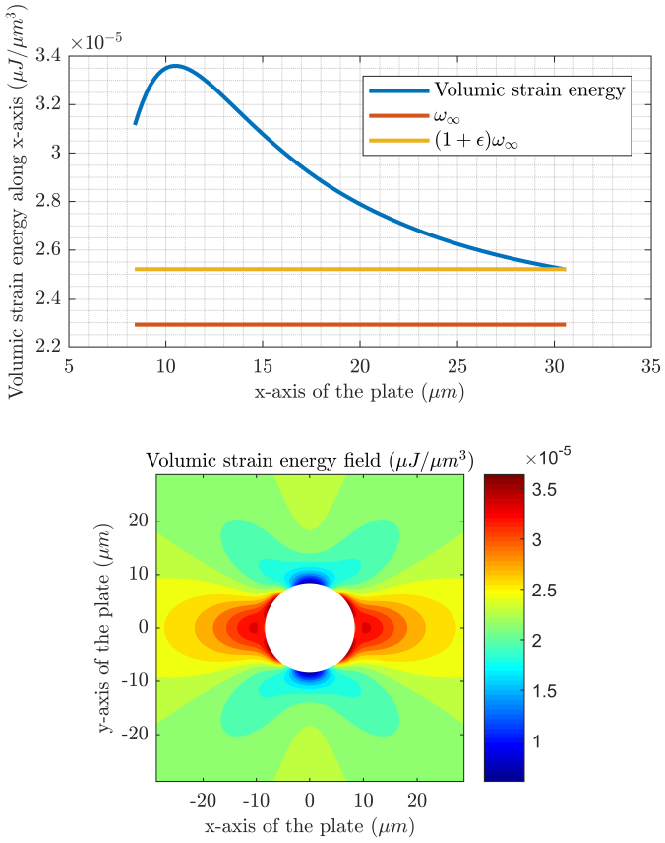

Fig. 19. Variations of the volumic strain energy along x-axis for a tensile test of amplitude σ^{∞}_{xx}. For $\mathbf{x}.\boldsymbol{x} = \dfrac{c}{2}$ the calculated energy reaches $(1+\epsilon)\omega_\infty$.

5.3. Numerical results

Once the *Handbook* has been defined, one wishes to reproduce the reference structure defined in Fig. 15. For that purpose the different enriched patterns are positioned on a macroscopic finite element mesh with the procedure described in the last point of Section 4, patterns with one or two fibers are arranged as shown in Fig. 20. Since the patterns have been prefabricated upstream it is not possible

to respect the identical arrangement of the fibers on the reference structure, this will lead to a first error when comparing the reference field with the field resulting from the MS-GFEM calculation. However this is not a problem in practice since the arrangement of the fibers is random, it is simply necessary to respect the volume fraction of the different components of the CMC. Moreover by observing Fig. 20 more carefully it is possible to anticipate bad interactions between the fibers. Indeed some features are missing in order to take into account all the interactions between fibers. Eventually some patterns overlap in part which will have the effect of accumulating local enrichments.

The macroscopic structure has a larger volume than the reference REV caused by the necessity of containing entirely the features and their support. Indeed the *Embedded Element* function is reliable if the nodes with interpolated displacements are located inside the master structure. To find conditions at the limits similar to those of the reference problem, the homogeneous strain is the same for the new model. The number of degrees of freedom is 708 for this model, it is about a thousand times less than for the finite element model.

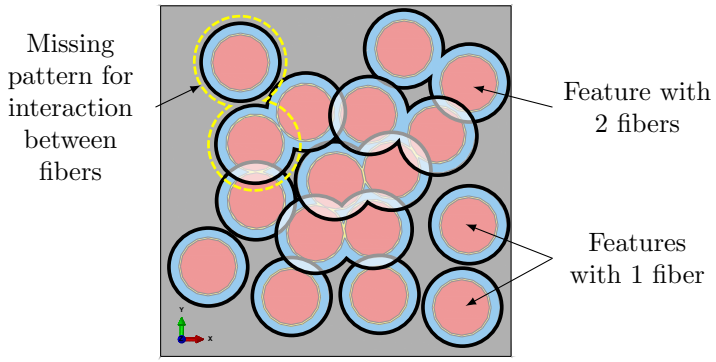

Fig. 20. Patterns arrangement in order to recreate the reference REV. Features with one or two fibers are used, they may also partially overlap each other.

The simulation enables to obtain the strain fields on each patch, nonetheless Abaqus tools do not allow to visualize on a common support the different contributions resulting from the patterns involved in the model. A first idea consists

in projecting the contributions of the enriched patterns onto a grid with the Abaqus function *Submodel*. However one comes back to the problem of field projection stated in the assessment of the difficulties related to the calculation of the GFEM stiffness matrix: such additional resolution is potentially costly. Then a second idea is to convert the strain fields into a color map so the color of a pixel is associated with a value of a component of the strain tensor. To realize the color map of each patch the Matlab software is used. The strain field is extracted from Abaqus in order to be recreated in Matlab. It turns out that image generation from fields is effective in Abaqus, hence its use. Fig. 21 shows a sample of the first component of the strain tensor calculated for three patches and their equivalent in terms of color map. A resolution of 512 colors is chosen and the color scale is calculated from the strain scale which explains why the colors around the fibers are different for the three patches.

After removing the homogeneous contribution in the strain tensor, the color maps can be summed in order to superimpose the enrichments. Once this step is completed, a rescaling can be made to add the homogeneous part of the strain. The result of this operation is illustrated in Fig. 22. It can be noticed that the range of values taken by the strains is wider than that of the reference calculation. This is explained by the superposition of enrichments when two features are locally overlaid as visible in Fig. 20. Nevertheless there is a correspondence between the location of the strain maxima for the reconstructed model and for the reference model. It is also possible to visualize the strain difference $\epsilon_{11}^{(gap)}$ between the reference strain field denoted $\epsilon_{11}^{(ref)}$ and the MS-GFEM one denoted $\epsilon_{11}^{(MS-GFEM)}$:

$$\epsilon_{11}^{(gap)} = \epsilon_{11}^{(ref)} - \epsilon_{11}^{(MS-GFEM)} \tag{19}$$

The $\epsilon_{11}^{(gap)}$ is shown in Fig. 23. The greatest visible differences correspond to the areas where the patterns overlap in Fig. 20. This result was already anticipated earlier in the article. Other gaps are calculated at the edges. These differences are caused by (i) strain jumps between the different phases (ii) the

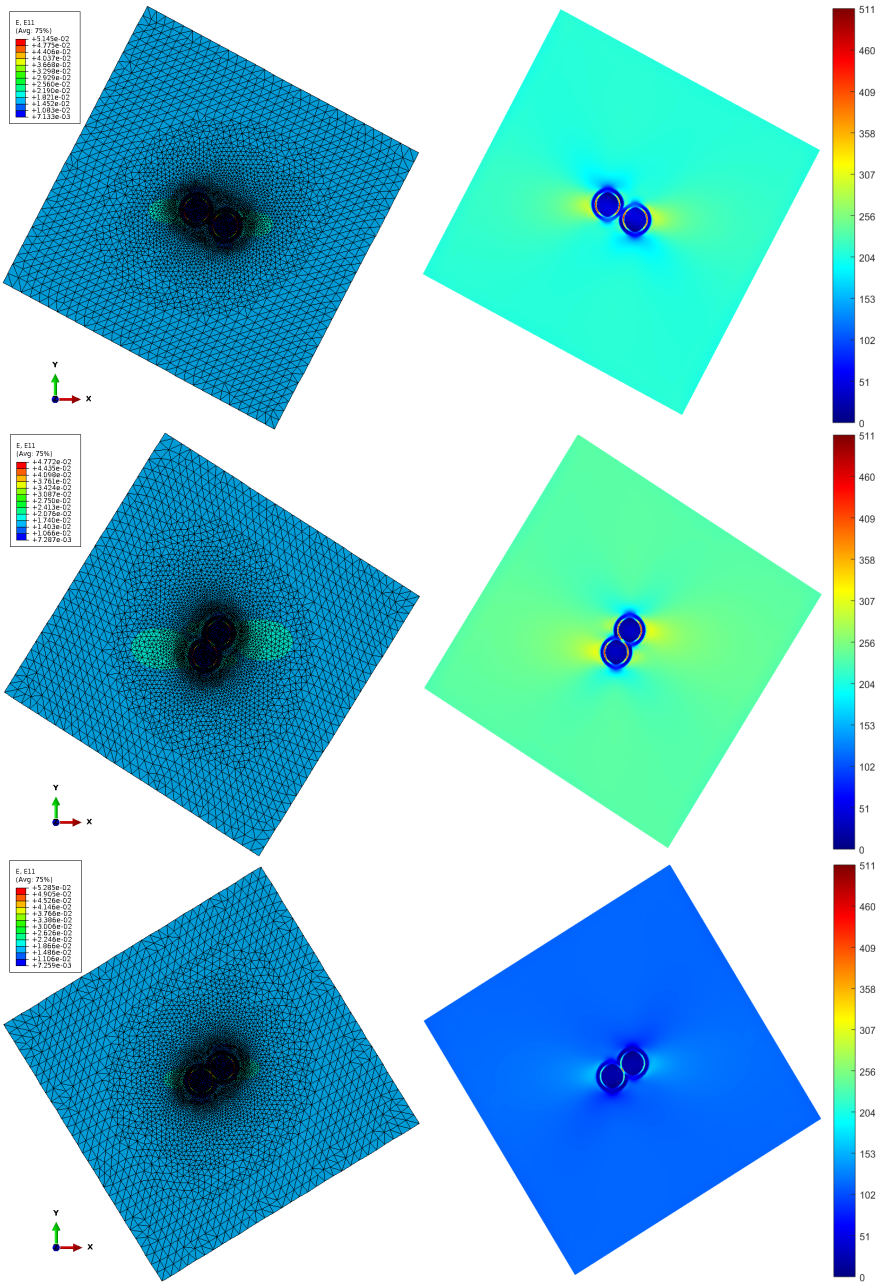

Fig. 21. Example of the conversion of the Abaqus strain field into a color map with a resolution of 512 colors. Each color scale is adapted from the strain scale.

impossibility of having identical meshes between the reference structure and the feature-generated structure (iii) the slight possible offset between the fibers of the reference model and the fibers of the reconstructed model. The relative gap is also proposed in Fig. 24, it can be noticed that the maximum error calculated is greater than 400% in some very localized areas. In order not to overwrite the the color scale a thresholded colormap is suggested in Fig. 25. As illustrated in Fig. 26, far from the edges the relative absolute error is less than 10% in the matrix, the interphase or the fiber and the error is higher in the zones of superimposed features. This last example points the importance of the patterns choice to minimize the error made in the reconstruction of the structure.

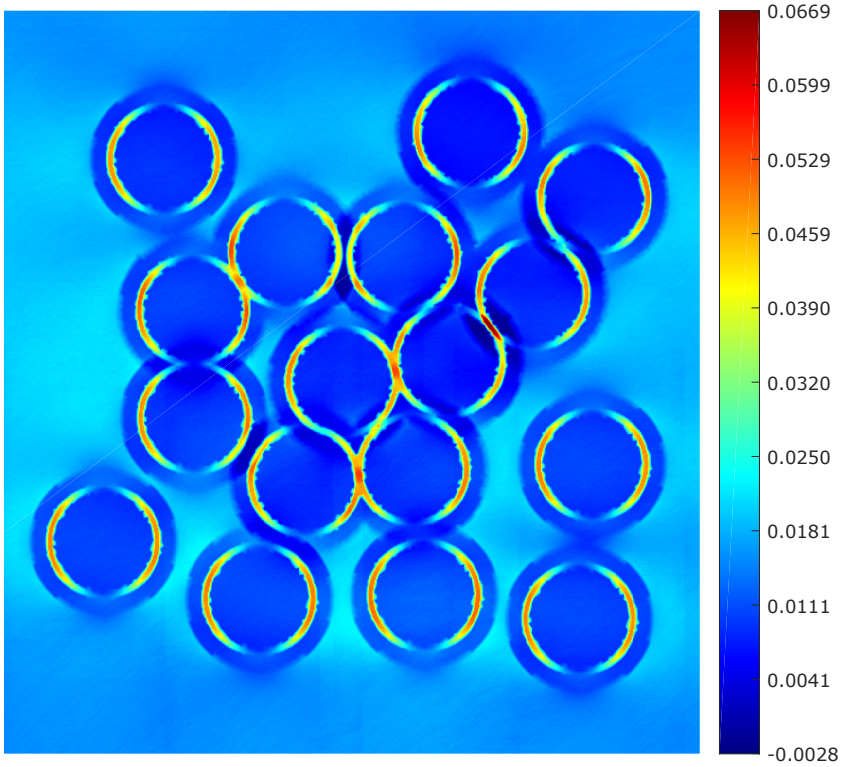

Fig. 22. Strain field obtained after the post-treatment of all the contributions of the patches, for the second positioning. The color bar scale given corresponds to the strain recalculated from the color maps of the different patterns.

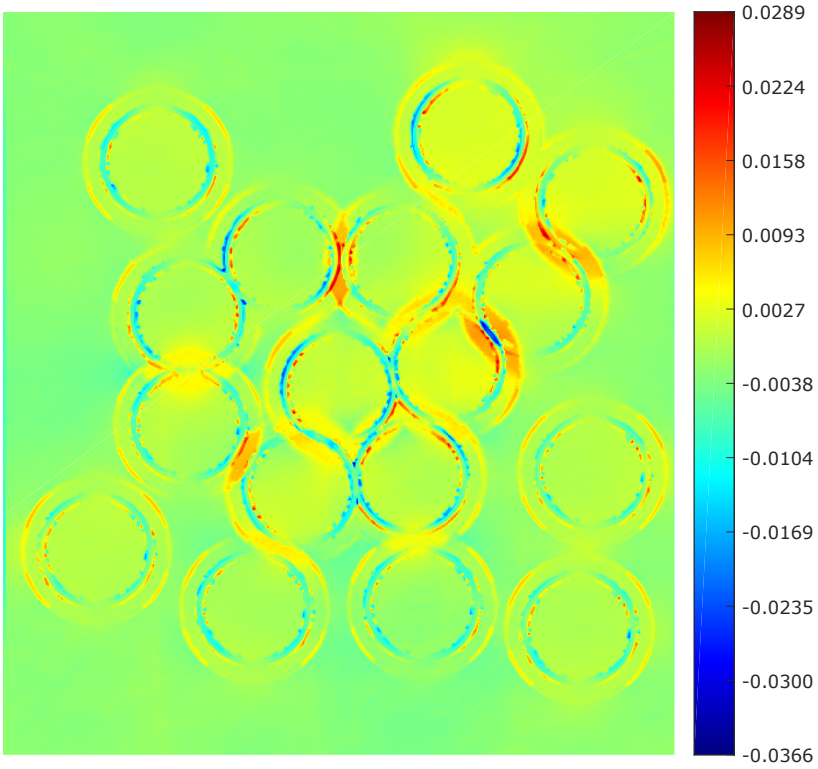

Fig. 23. Field gap obtained from the reference strain field and the MS-GFEM one. The greatest gaps are located in non-empty intersections between features. Other gaps are visible at the edges due to the Matlab post-treatment.

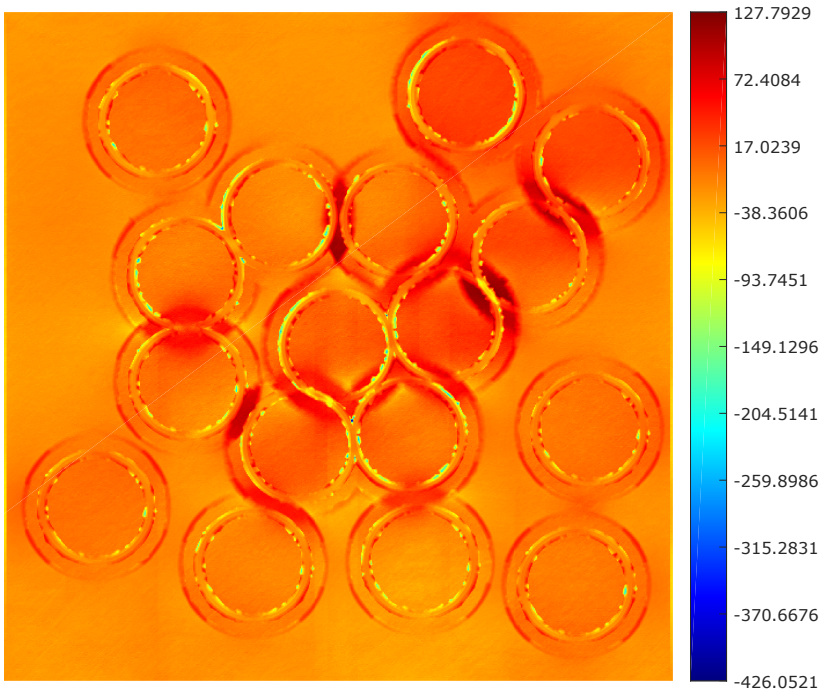

Fig. 24. Relative field gap (%)

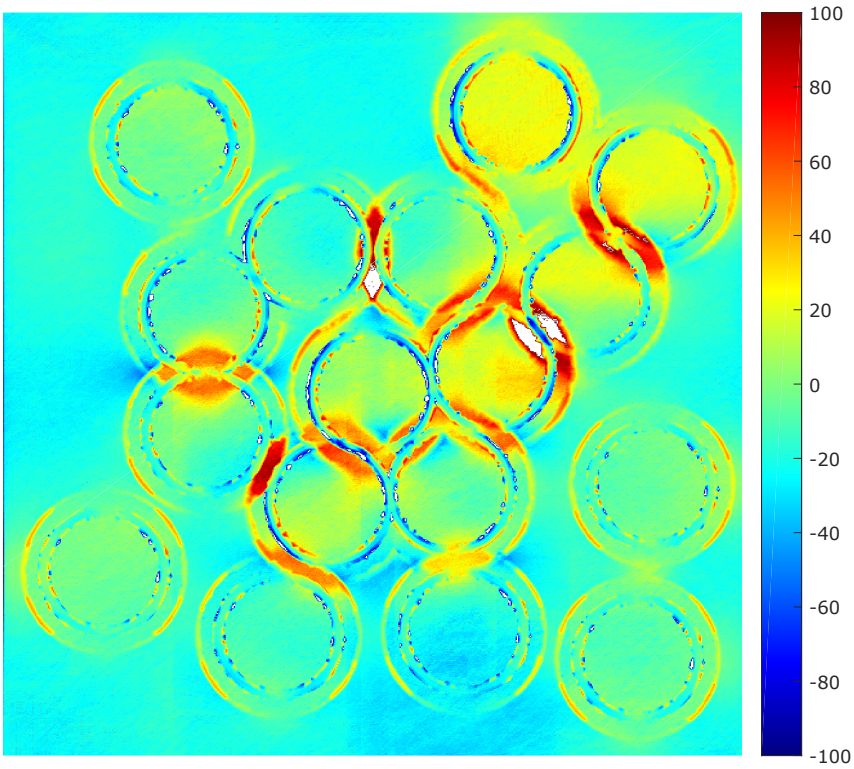

Fig. 25. Relative field gap (%) with a threshold in order not to overwrite the color scale. The white zones are defined as "Not a Number" and refer to the errors higher than 100% in absolute value.

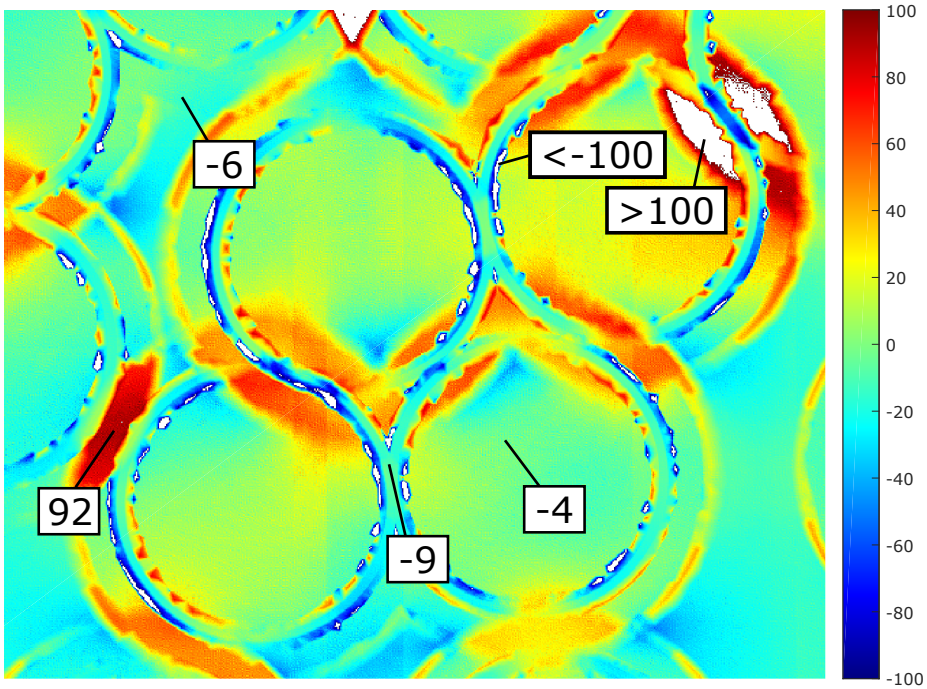

Fig. 26. Values of interest picked in the relative gap map (values in %).

6. Conclusion

This paper has shown the possibility of the numerical implementation of two GFEM strategies within the Abaqus software. A discussion has been conducted in order to select the most versatile method regarding the desire to develop a tool for CMC micro-structures description. Then an application of the MS-GFEM to a micro-structure of a CMC has been made in an elastic problem. It can be noticed that the presented Abaqus tools can also be used to build the Duarte's GFEM.

It has been shown that Abaqus possesses functionalities to (i) generate numerical enrichment functions with regard to the MS-GFEM hypotheses (ii) interpolate a macroscopic kinematics on non-interacting patches which contain structural detail information.

In term of current limitations, two can be noted. First in the MS-GFEM strategy it is important to keep in mind the time allocated to search for the location of patches files and read the associated information during a simulation. Then the time gain due to the limited degrees of freedom is partially compensated with that additional operation. Consequently the MS-GFEM is worthwhile in the case of a rich structure modeling which would demand a very fine mesh if treated by a classic finite element method. Fortunately in the case of a CMC description many structural details must be taken into account and the MS-GFEM becomes a relevant strategy to study such materials, at the condition of an appropriate choice of the patterns and their placement. Secondly the Abaqus substructuring tool gives a representation of a linear and static behavior of a selected volume. Consequently extra researches must be led to take into account non-linear phenomena, a first step in this direction is presented in [52]. Eventually the choice in the patch positioning must be made carefully not to accumulate the perturbation functions describing a common feature.

Some perspectives can be highlighted. First investigations concerning the automation of patterns selection could be carried out based on the observation of real microstructures and automatic learning algorithms. The objective would

then be to obtain more complex but more representative patterns of the composite while keeping as much as possible the versatile aspect of the GFEM method. Secondly iterative enrichments could be considered in order to update the state of each patch and to integrate degradation mechanisms such as crack propagation or creep under high temperatures. Numerical methods like POD can be considered as suggested in [47]. Eventually statistical and random aspects such as the variability of the fibers radius or the respect of the rates (of porosity, fibers, matrix) can also be taken into account in order to distribute the patterns while respecting the representative character of observable micro-structures.

Acknowledgements

The authors wish to acknowledge the support of Safran Ceramics and the ANRT for funding this research.

References

References

[1] F. W. Zok, Ceramic-matrix composites enable revolutionary gains in turbine engine efficiency, Am Ceram Soc Bull 95 (5) (2016) 22–8.

[2] G. Corman, K. Luthra, Development history of GE's prepreg melt infiltrated ceramic matrix composite material and applications, Computer methods in applied mechanics and engineering (2017).

[3] A. Pryce, P. Smith, Behaviour of unidirectional and crossply ceramic matrix composites under quasi-static tensile loading, Journal of materials science 27 (10) (1992) 2695–2704.

[4] R. Yamada, T. Taguchi, N. Igawa, Mechanical and thermal properties of 2D and 3D SiC/SiC composites, Journal of nuclear materials 283 (2000) 574–578.

[5] P. Boisse, Textile reinforcements: Architectures, mechanical behavior, and forming, Ceramic Matrix Composites: Materials, Modeling and Technology (2014) 65–84.

[6] W. Yang, L. Zhang, Y. Liu, L. Cheng, W. Zhang, Preparation and mechanical properties of carbon fiber reinforced (bc x–SiC) n multilayered matrix composites, Applied Composite Materials 14 (4) (2007) 277–286.

[7] J. Brennan, Interfacial characterization of a slurry-cast melt-infiltrated SiC/SiC ceramic-matrix composite, Acta materialia 48 (18-19) (2000) 4619–4628.

[8] J. A. DiCarlo, Advances in SiC/SiC Composites for Aero-Propulsion, The American ceramic society, 2013, Ch. 7, pp. 217–235.

[9] A. Evans, F. Zok, The physics and mechanics of fibre-reinforced brittle matrix composites, Journal of Materials science 29 (15) (1994) 3857–3896.

[10] A. G. Evans, F. W. Zok, R. M. McMeeking, Z. Z. Du, Models of high-temperature, environmentally assisted embrittlement in ceramic-matrix composites, Journal of the American Ceramic Society 79 (9) (1996) 2345–2352.

[11] F. Abbé, Flexural creep behavior of a 2D SiC/SiC composite, Ph.D. thesis, Ph. D. thesis, University of Caen (1990).

[12] P. Carrère, J. Lamon, Creep behaviour of a SiC/Si-BC composite with a self-healing multilayered matrix, Journal of the European Ceramic Society 23 (7) (2003) 1105–1114.

[13] V. Herb, G. Couégnat, E. Martin, Damage assessment of thin SiC/SiC composite plates subjected to quasi-static indentation loading, Composites Part A: Applied Science and Manufacturing 41 (11) (2010) 1677–1685.

[14] V. Herb, E. Martin, G. Couégnat, Damage analysis of thin 3D-woven SiC/SiC composite under low velocity impact loading, Composites Part A: Applied Science and Manufacturing 43 (2) (2012) 247–253.

[15] J.-L. Bobet, J. Lamon, Study of thermal residual stresses in ceramic matrix composites, Journal of alloys and compounds 259 (1-2) (1997) 260–264.

[16] H. Mei, Measurement and calculation of thermal residual stress in fiber reinforced ceramic matrix composites, Composites science and technology 68 (15-16) (2008) 3285–3292.

[17] J.-L. Bobet, J. Lamon, Thermal residual stresses in ceramic matrix composites—i. axisymmetrical model and finite element analysis, Acta metallurgica et materialia 43 (6) (1995) 2241–2253.

[18] P. Pineau, G. Couégnat, J. Lamon, Virtual testing applied to transverse multiple cracking of tows in woven ceramic composites, Mechanics Research Communications 38 (8) (2011) 579–585.

[19] V. Mazars, G. Couégnat, O. Caty, S. Denneulin, G. Vignoles, Multi-scale damage modeling of 3D ceramic matrix composites from in-situ X-ray tensile tests, in: ECCM18, 2018, pp. 24–28.

[20] F. Pailler, J. Lamon, Micromechanics based model of fatigue/oxidation for ceramic matrix composites, Composites science and technology 65 (3-4) (2005) 369–374.

[21] S. Nemat-Nasser, Overall stresses and strains in solids with microstructure, in: Modelling Small Deformations of Polycrystals, Springer, 1986, pp. 41–64.

[22] E. Sanchez-Palencia, Homogenization method for the study of composite media, in: Asymptotic Analysis II—, Springer, 1983, pp. 192–214.

[23] J. Fish, K. Shek, Multiscale analysis of composite materials and structures, Composites Science and Technology 60 (12-13) (2000) 2547–2556.

[24] F. Feyel, Multiscale FE2 elastoviscoplastic analysis of composite structures, Computational Materials Science 16 (1-4) (1999) 344–354.

[25] L. Gélébart, R. Mondon-Cancel, Non-linear extension of FFT-based methods accelerated by conjugate gradients to evaluate the mechanical behavior of composite materials, Computational Materials Science 77 (2013) 430–439.

[26] P. Ladeveze, Multiscale modelling and computational strategies for composites, International Journal for Numerical Methods in Engineering 60 (1) (2004) 233–253.

[27] J. Guo, D. Shi, Q. Wang, F. Pang, Q. Liang, A domain decomposition approach for static and dynamic analysis of composite laminated curved beam with general elastic restrains, Mechanics of Advanced Materials and Structures (2018) 1–13.

[28] P.-A. Guidault, O. Allix, L. Champaney, C. Cornuault, A multiscale extended finite element method for crack propagation, Computer Methods in Applied Mechanics and Engineering 197 (5) (2008) 381–399.

[29] J. Fish, The s-version of the finite element method, Computers & Structures 43 (3) (1992) 539–547.

[30] C. A. Duarte, J. T. Oden, An hp adaptive method using clouds, Computer methods in applied mechanics and engineering 139 (1-4) (1996) 237–262.

[31] J. M. Melenk, I. Babuška, The partition of unity finite element method: basic theory and applications, Computer methods in applied mechanics and engineering 139 (1-4) (1996) 289–314.

[32] T. Strouboulis, I. Babuška, K. Copps, The design and analysis of the generalized finite element method, Computer methods in applied mechanics and engineering 181 (1) (1998) 43–69.

[33] M. Fleming, Y. Chu, B. Moran, T. Belytschko, Enriched element-free galerkin methods for crack tip fields, International journal for numerical methods in engineering 40 (8) (1997) 1483–1504.

[34] D. Shepard, A two-dimensional interpolation function for irregularly-spaced data, in: Proceedings of the 1968 23rd ACM national conference, ACM, 1968, pp. 517–524.

[35] C. Duarte, O. Hamzeh, T. Liszka, W. Tworzydlo, A generalized finite element method for the simulation of three-dimensional dynamic crack propagation, Computer Methods in Applied Mechanics and Engineering 190 (15-17) (2001) 2227–2262.

[36] A. M. Aragón, C. A. Duarte, P. H. Geubelle, Generalized finite element enrichment functions for discontinuous gradient fields, International Journal for Numerical Methods in Engineering 82 (2) (2010) 242–268.

[37] M. Braginsky, C. Przybyla, Simulation of crack propagation/deflection in ceramic matrix continuous fiber reinforced composites with weak interphase via the extended finite element method, Composite Structures 136 (2016) 538–545.

[38] H. Talebi, M. Silani, S. P. Bordas, P. Kerfriden, T. Rabczuk, A computational library for multiscale modeling of material failure, Computational Mechanics 53 (5) (2014) 1047–1071.

[39] G. Zi, T. Belytschko, New crack-tip elements for xfem and applications to cohesive cracks, International Journal for Numerical Methods in Engineering 57 (15) (2003) 2221–2240.

[40] T. Menouillard, J. Rethore, A. Combescure, H. Bung, Efficient explicit time stepping for the extended finite element method (X-FEM), International Journal for Numerical Methods in Engineering 68 (9) (2006) 911–939.

[41] T.-P. Fries, A corrected XFEM approximation without problems in blending elements, International Journal for Numerical Methods in Engineering 75 (5) (2008) 503–532.

[42] S. P. Bordas, S. Natarajan, P. Kerfriden, C. E. Augarde, D. R. Mahapatra, T. Rabczuk, S. D. Pont, On the performance of strain smoothing for quadratic and enriched finite element approximations (XFEM/GFEM/PUFEM), International Journal for Numerical Methods in Engineering 86 (4-5) (2011) 637–666.

[43] J.-Y. Wu, F.-B. Li, An improved stable XFEM (Is-XFEM) with a novel enrichment function for the computational modeling of cohesive cracks, Computer Methods in Applied Mechanics and Engineering 295 (2015) 77–107.

[44] C. A. Duarte, D.-J. Kim, Analysis and applications of a generalized finite element method with global–local enrichment functions, Computer Methods in Applied Mechanics and Engineering 197 (6) (2008) 487–504.

[45] T. Strouboulis, K. Copps, I. Babuška, The generalized finite element method, Computer methods in applied mechanics and engineering 190 (32) (2001) 4081–4193.

[46] T. Strouboulis, L. Zhang, I. Babuška, Generalized finite element method using mesh-based handbooks: application to problems in domains with many voids, Computer Methods in Applied Mechanics and Engineering 192 (28-30) (2003) 3109–3161.

[47] W. Aquino, J. Brigham, C. Earls, N. Sukumar, Generalized finite element method using proper orthogonal decomposition, International journal for numerical methods in engineering 79 (7) (2009) 887–906.

[48] D. Canales, A. Leygue, F. Chinesta, D. González, E. Cueto, E. Feulvarch, J.-M. Bergheau, A. Huerta, Vademecum-based GFEM (V-GFEM): optimal enrichment for transient problems, International Journal for Numerical Methods in Engineering 108 (9) (2016) 971–989.

[49] I. Babuška, U. Banerjee, Stable generalized finite element method (SGFEM), Computer Methods in Applied Mechanics and Engineering 201 (2012) 91–111.

[50] V. Gupta, C. A. Duarte, I. Babuška, U. Banerjee, A stable and optimally convergent generalized FEM (SGFEM) for linear elastic fracture mechanics, Computer methods in applied mechanics and engineering 266 (2013) 23–39.

[51] B. Tranquart, P. Ladevèze, E. Baranger, A. Mouret, A computational approach for handling complex composite microstructures, Composite Structures 94 (6) (2012) 2097–2109.

[52] O. Friderikos, E. Baranger, P. Ladevèze, Multiscale gfem with superposition of crack enrichment functions driven by finite fracture mechanics: Theory, first computation and open problems, Composite Structures 164 (2017) 145–157.

[53] D. Dunn, The effect of fiber volume fraction in HiPerComp® SiC-SiC composites, Ph.D. thesis, New York State College of Ceramics at Alfred University. (2010).

[54] http://www.coiceramics.com/pdfs/Hi-Nicalon-Type-S.pdf.

[55] R. R. Naslain, R. J.-F. Pailler, J. L. Lamon, Single-and multilayered interphases in SiC/SiC composites exposed to severe environmental conditions: an overview, International Journal of Applied Ceramic Technology 7 (3) (2010) 263–275.

[56] Y. Katoh, K. Ozawa, C. Shih, T. Nozawa, R. J. Shinavski, A. Hasegawa, L. L. Snead, Continuous SiC fiber, CVI SiC matrix composites for nuclear applications: Properties and irradiation effects, Journal of Nuclear Materials 448 (1-3) (2014) 448–476.

[57] S. G. Lekhnitskii, Anisotropic plates, Tech. rep., Foreign Technology Div Wright-Patterson Afb Oh (1968).

[58] J. Dundurs, Mathematical theory of dislocations, American Society of Mechanical Engineers (ASME), New York (1969) 70–115.

Appendix 1

If $\boldsymbol{u}_h = \boldsymbol{u}_{FEM} + \boldsymbol{u}_{enr}$ denotes the GFEM kinematics as the sum of the classical finite element displacement $\boldsymbol{u}_{FEM}$ and the enriched contribution $\boldsymbol{u}_{enr}$ and $\boldsymbol{u}_h^* = \boldsymbol{u}_{FEM}^* + \boldsymbol{u}_{enr}^*$ denotes the associated virtual field the virtual work of the internal forces can be developed as:

$$
\begin{aligned}
& \int_\Omega \mathbf{H}(\underline{x})\underline{\underline{\epsilon}}(\boldsymbol{u}_h) : \underline{\underline{\epsilon}}(\boldsymbol{u}_h^*) d\Omega \\
= & \int_\Omega \mathbf{H}(\underline{x})\underline{\underline{\epsilon}}(\boldsymbol{u}_{FEM}) : \underline{\underline{\epsilon}}(\boldsymbol{u}_{FEM}^*) d\Omega \\
+ & \int_\Omega \mathbf{H}(\underline{x})\underline{\underline{\epsilon}}(\boldsymbol{u}_{enr}) : \underline{\underline{\epsilon}}(\boldsymbol{u}_{enr}^*) d\Omega \\
+ & \int_\Omega \mathbf{H}(\underline{x})\underline{\underline{\epsilon}}(\boldsymbol{u}_{FEM}) : \underline{\underline{\epsilon}}(\boldsymbol{u}_{enr}^*) d\Omega \\
+ & \int_\Omega \mathbf{H}(\underline{x})\underline{\underline{\epsilon}}(\boldsymbol{u}_{enr}) : \underline{\underline{\epsilon}}(\boldsymbol{u}_{FEM}^*) d\Omega
\end{aligned}
$$

The Voigt convention gives $\underline{\underline{\epsilon}}(\boldsymbol{u}_{FEM}) = \underline{U}_{FEM}\underline{B}_{FEM}^T$ and $\underline{\underline{\epsilon}}(\boldsymbol{u}_{enr}) = \underline{U}_{enr}\underline{B}_{enr}^T$ where $\underline{A}^T$ is the transpose tensor of column vector A. Coordinates of the displacement vectors are given by $(\underline{U}_{FEM})_I = \boldsymbol{u}_I$, $(\underline{U}_{enr})_\alpha = \boldsymbol{a}_p^k$ where $\alpha = \sum_{m=1}^{p-1} n_{enr}^{(m)} + k$ and $\left(\underline{B}_{FEM}^T\right)_I = \nabla(\varphi_I)$, $\left(\underline{B}_{enr}^T\right)_\beta = \nabla(\varphi_q \psi_q^{(l)})$ where $\beta = \sum_{n=1}^{q-1} n_{enr}^{(n)} + l$. As a convention if the index p (respectively q) in the expression of α (respectively β) equals 1 it is assumed that $\alpha = k$ (respectively $\beta = l$). Since the hat functions φ_k are not equal to zero only on the patch Ω_k the domains of integration are reduced to the ones precised in (9).

Appendix 2

1

Macroscopic shape functions φ_k ($k \in [\![1; n]\!]$) projected on the local mesh, on each local node i the value is denoted $\varphi_k^{(i)}$

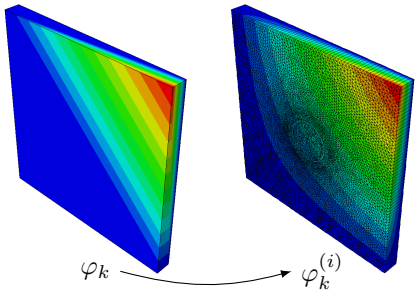

2.1

Canonical strain basis $\widehat{\underline{\underline{\epsilon}}}$ applied on a refined mesh:

1. with a homogeneous behavior
2. with the structural detail behavior

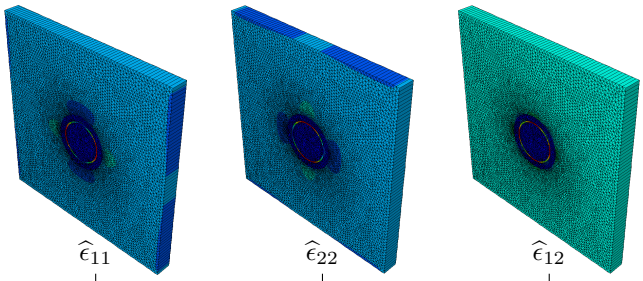

2.2

Generation of 6 enrichment functions associated to each load case by deleting the homogeneous part from the patch. On each local node i one gets $\psi_j^{(i)}$

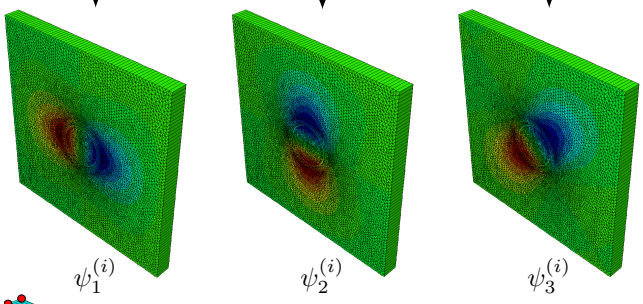

3

GFEM kinematics imposed to each local node $\boldsymbol{u}_i^{(local)}$

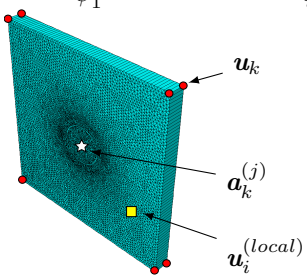

4

Substructuring on the macroscopic nodes $\boldsymbol{u}_k$ and $\boldsymbol{a}_k^{(j)}$

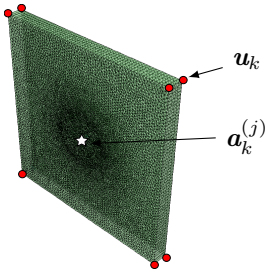

5

Patch positioning on a macroscopic finite element support